Published in JOURNAL OF GEOPHYSICAL RESEARCH, VOL. 108, NO. C12, 3390, doi:10.1029/2002JC001610, 2003

Dense Water Cascading off the Continental Shelf

G.I.Shapiro(1,3), J.M.Huthnance(2), V.V.Ivanov(1)

1- Institute of Marine Studies, University of Plymouth, UK

2- Proudman Oceanographic Laboratory, Bidston, UK

3- Shirshov Institute of Oceanology, Moscow, Russia

Submitted to Journal of Geophysical Research *July 2002*

Revised 16/04/2003

Corresponding author:

Prof G I Shapiro
Institute of Marine Studies,
University of Plymouth,
Drake Circus,
Plymouth,
PL4 8AA, UK,
email: g.shapiro@plymouth.ac.uk,
tel: +44-(0)1752-232423,
fax:+44-(0)1752-232406

ABSTRACT

Cascading is a specific type of buoyancy driven current, in which dense water formed by cooling, evaporation or freezing in the surface layer over the continental shelf descends down the continental slope to a greater depth. We have identified, by world-wide trawling and analysis of raw data bases, several distinct mechanisms of pre-conditioning for cascades. We have validated, where possible, existing theories and developed simple models, which allow estimation of the parameters for pre-conditioning, initiating and down-slope fluxes as well as evolution of the temperature contrasts during cascading events. Compliance or non-compliance of observations with these simple and easy-to- use models has been related to the stage of cascade development and to local factors. Estimates of observed down-slope transport rates in case studies accord with theory, which is thereby substantially validated. Typical values of cascading transport rates were in the range 0.5 – 1.6 m^2s^{-1}. We hazard a very approximate global estimate of order 10^5 km^3yr^{-1} or average 3 Sv, based on our findings and previous studies.

1. INTRODUCTION

Cascading is a specific type of buoyancy driven current, in which dense water formed by cooling, evaporation or freezing in the surface layer over the continental shelf descends down the continental slope to a greater depth. This process is a major component of ventilation of intermediate and abyssal waters, hence affecting thermohaline circulation (Killworth, 1983) and global climate (Meincke et al., 1997). Dense water can be produced more effectively in shallow areas of the continental shelf than in the adjacent deep waters, and eventually spills over the shelf edge onto the steeper continental slope (Nansen, 1913, Cooper and Vaux, 1949, Huthnance, 1995, Shapiro and Hill, 1997). The resulting flows produce an irreversible exchange of oceanic and shelf waters (Whitehead, 1987; Huthnance, 1995) and take an important role in bio-geochemical cycles by removal of phytoplankton, carbon (Yoder and Ishimaru, 1989) and chlorophyll (Hill et al., 1998) from productive areas. Because it can take decades or more for the subducted water to re-surface, water cascades contribute to long term climatic variability (Condie, 1995). Although there are no accurate estimates, it is believed that the turbidity currents transporting terrigenous material to the deep sea (Dade and Huppert, 1994) may be facilitated by cascading (Huthnance, 1995, Backhaus et al., 1997).

Large scale water cascades in the Antarctic ocean (Baines and Condie, 1998) lead to the formation of Antarctic Bottom Water (AABW), the most widespread water mass in the world. Dense water overflows off the vast Arctic shelves are crucial to maintaining and replenishing the Arctic Ocean Cold Halocline (Aagaard et al., 1981), a layer between 50-150 m deep which separates the cold surface layer from warmer, saltier and denser water entering from the North Atlantic. Sinking of dense water contributes to the formation of Arctic

Intermediate Waters (Rudels, 1986; Jones et al., 1995). Backhaus et al (1997) discussed the importance of shelf-origin, brine-enriched bottom waters in ventilating intermediate and deep layers of the Nordic Seas and the Arctic Ocean. This process eventually contributes to the shaping of the Atlantic Meridional Overturning Circulation (Turrell et al., 1999).

Despite its global importance, cascading is often an intermittent process (Huthnance, 1995), it is often composed of individual mesoscale events, it takes place in the bottom layers and cannot be traced using modern satellite technology; hence it is rarely observed while in progress. When the sources of dense water are variable in space and time, the resulting dense water masses are likely to take the form of mesoscale individual cold/salty lenses perched on the slope (Saunders, 1990) or dense plumes with significant 3-dimensional structure (Shapiro and Hill, 2003). Alternatively, dense water can propagate down-slope due to baroclinic instability of an along slope current, through formation of spiral waves, meanders and eddies (Whitehead et al., 1990; Condie, 1995; Shapiro and Zatsepin, 1997; Lane-Serff and Baines, 1998).

Deep water formation by the cascading process can be split in three stages, (i) dense water formation on the shelf, (ii) transport of source water to a greater depth along the sloping bottom, and (iii) mixing the new incoming water with the ambient waters at the equilibrium density level. In this paper we are mostly concerned with the first two stages, i.e. pre-conditioning and water cascading itself, with a brief discussion of fates. From the point of view of fluid dynamics, a dense water cascade is a type of gravity current, which propagates both along- and across-slope under the influence of gravity, Earth rotation, friction and entrainment (mixing). Despite recent progress in understanding the physics of dense water

overflow, through mathematical modelling and laboratory experiments (e.g. Lane-Serff, 2001 and references therein), dense water cascades represent a source of major uncertainty in ocean circulation and coupled climate models (Condie, 1995). There is a dearth of knowledge of the main individual characteristics of water cascades, most favourable locations, typical density difference, speed of sinking, off-shore volume fluxes etc.

The aim of this paper is three-fold. First, to identify differences in mechanisms of mesoscale water cascades by world-wide trawling of raw data bases. Second, to validate existing theories and, where possible, to develop a few simple equations for estimating cascading parameters, in an attempt to reflect various cascading mechanisms. Third, to infer, through application of model results, the parameters of cascading that are difficult to observe. The pre-conditioning stage of cascading is analysed in Section 2, while in Section 3 we discuss the features of down-slope propagation. Particular focus is on the estimation of the life span of individual water cascades in different climatic zones. Fates of cascaded plumes are discussed in Section 4 and the results are summarised in Section 5. A systematic inventory of cascading events with more than 60 confirmed cases will be published separately.

2. PRE-CONDITIONING

There are a few physical mechanisms for formation of horizontal density gradients in the bottom layer between shallow and deep waters, which are favourable for cascading. All the processes discussed in this paper include sea-air interactions and convective mixing in the surface layer due to atmospheric forcing. However these mechanisms differ in that the density contrast can be produced mainly by temperature, mainly by salinity, or by the combination of both. They may be facilitated or hampered by the formation of temperature and/or salinity fronts due to horizontal advection or tidal mixing.

In shallow areas, where the water depth is less than the depth of penetrating convection, caused by surface cooling, convective mixing tends to produce a nearly homogeneous mass of water. As there is a thinner layer of water to be cooled over the shelf than over the deep sea, the cooling will make the water colder and heavier than in the surrounding deeper regions (F.Nansen, 1906, 1913). Similar processes take place due to surface salinization of water caused by strong evaporation in summer or ice formation in winter. While based on salinity increase due to ice formation, cascading mechanisms are different in free-of-ice and ice-covered seas. In this section we analyse the physics of idealised basic mechanisms, each being illustrated by one example of observed cascading events.

2.1. Temperature driven cascades

This sub-section is concerned with the mechanisms in which local temperature response to winter cooling is the major driver of the cascade, while other processes, such as advection of temperature and/or salinity may or may not have a significant role. If the convection depth exceeds the depth of the shelf, then a density difference is formed between the shelf and offshore waters. Following Symonds and Gardiner-Garden (1994) let us assume that (i) meteorological conditions and hence the outward buoyancy fluxes are the same for the shelf region and adjacent deep water; (ii) convective cooling initially produced a uniform mixed layer H_S equal to the depth of the shelf; (iii) the temperature gradient, dT/dz, in deep waters below the mixed layer is constant; (iv) the contribution of salinity to density is negligible; (v) there is no horizontal advection. Further cooling and deepening of the convective layer off-shore results in the temperature difference between the shelf and off-shore waters, see Fig.1:

$$\Delta T = T_c - T_s = \frac{1}{2}\frac{dT}{dz}\frac{(H_c - H_s)^2}{H_s} \qquad (1)$$

where subscripts *s, c* correspond to the shelf and offshore convective layers respectively; Hc is the final depth of the offshore mixed layer. If an initial temperature difference exists between shallow and deep waters it can be added to the value given by eq. (1).

This theory can be generalised to include a salinity gradient, *dS/dz*, below the convective layer. If a salinity gradient is present, convective mixing (driven by surface cooling) produces salinity and temperature jumps at the bottom of the mixed layer in deep water. A stable salinity gradient gives rise to formation of an intermediate warm layer and temperature inversion (Zubov, 1947). Further deepening is only possible when the mixed layer is cooled enough that the discontinuity in the vertical profiles of temperature and salinity does not result in discontinuity of water density (Fig.1). Assuming that no precipitation or salinisation occurs and equating heat fluxes over the shelf and deep waters one can obtain

$$\Delta T = T_c - T_s = \frac{1}{2}\frac{dT}{dz}\frac{(H_c - H_s)^2}{H_s} - \frac{\beta}{2\alpha}\frac{dS}{dz}\frac{(H_c - H_s)^2(H_c + H_s)}{H_c H_s} \qquad (2)$$

$$\Delta S = S_c - S_s = -\frac{1}{2}\frac{dS}{dz}\frac{(H_c - H_s)^2}{H_c} \qquad (3)$$

$$\Delta \rho = \rho_c - \rho_s = (\beta\frac{dS}{dz} - \alpha\frac{dT}{dz})\frac{(H_c - H_s)^2}{2H_s} \qquad (4),$$

where $\alpha/\rho>0$ is the thermal expansion coefficient; $\beta/\rho>0$ is the salinity contraction coefficient.

Non-local effects, i.e. horizontal advection of temperature and/or salinity can enhance or decrease the density contrasts. However the horizontal advection on its own, without contribution from local vertical mixing due sea-air interaction is not able to generate conditions favourable for cascading. Examples of different pre-conditioning mechanisms involving temperature response to local cooling are given below.

A. Temperature response to cooling of surface waters, no horizontal advection

Thermohaline structure over the north-west European shelf/slope between the Celtic Sea in the south and the Faeroe Isles in the north (Fig. 2) is favourable for cascading and features strong annual temperature variability, exceeding 5^0C at the surface. Seasonal variability in salinity, caused by evaporation and precipitation, is very small and does not normally exceed 0.10 PSU (Ellett et al., 1986). Relative contributions of temperature and salinity to density changes at the surface can be as high as R_ρ = 10:1. Hence potential water cascades are likely to be driven by seasonal cooling.

Cascading events have been repeatedly observed near Rockall Bank west of Ireland. Fig. 3 shows a transect across Rockall Bank (Nansen, 1913) - the first direct observation of cascading. The average depth of the bank is Hs=150m, and the seabed rapidly descends to 1500-2500m away from the bank. Summer observations (Fig. 3) show cold dense water sinking and spreading away from the bank. Nansen estimated the depth of dense water

penetration from the previous winter as 400-600m referring to nearly homogeneous density around the Bank within the layer 200-600m and the shape of the isopycnal σ_θ= 27.40. On the west side, the depth of the nearly homogeneous layer is about 400 m (measured by the depth of the isopycnal σ_θ= 27.40); in the Rockall trough, water of the same density is as deep as 800m, which could be attributed to cascading from the top of the bank. From the data shown in Fig 3 it follows that the observed values for the temperature, salinity and density contrasts at 200 m are $\Delta T=T_c-T_s=0.75\ ^oC$, $\Delta S=S_c-S_s=0.04$ PSU , $\Delta\rho=\rho_c-\rho_s$ = -0.09 kg/m^3, density ratio is $R_\rho=(-\alpha\Delta T)/(\beta\Delta S)$ =(-0.12)/(0.03).

Figs.4,5 show similar transects occupied in July, 1966 and January 1967 (Ellett, 1968). By the end of January 1967 the convection depth on both sides of Rockall Bank was about Hc=500m. Mean vertical temperature and salinity gradients in the layer 150-500m in the previous summer were $dT/dz=1.8x10^{-3}$(°C/m) and $dS/dz=0.3x10^{-4}$(PSU/m). Other observed parameters are T_s=8.4, T_c=9.15°C, S_c=35.38 PSU, same salinity on the shelf S_s=35.38PSU, ρ_c=27.39, ρ_s=27.51 kgm^3. Calculations with Eqs (2) - (4) predict the following values for the temperature and density contrasts during cascading, ΔT=0.66°C and $\Delta\rho$ =-0.11 kg/m^3; the predicted density ratio is R_ρ=(-0.11)/(-0.03). The observed values at 150 m are ΔT=0.75°C, $\Delta\rho$=-0.12 kg/m3 and R_ρ=(-0.12)/(0.0), are in good agreement with their theoretically predicted counterparts. A good coincidence between the observed and predicted values validates the use of equations (2) – (4) and supports the hypothesis that the cascading is driven by enhanced local cooling over the shelf.

B. Temperature response to surface cooling assisted by advection of salinity

A good example of how horizontal advection can facilitate cascading is the Malin cascade (Hill et al., 1998). Down-slope protrusion of warm and saline water, which extended to a depth of 500m, was observed in February 1996 off the Malin shelf (Fig. 6); cascading of shelf waters was substantiated by chlorophyll and dissolved oxygen measurements. The saline water over the Malin shelf is provided by the Rockall Slope Current, which carries warmer and saltier water northwards (Huthnance, 1986). As argued by Hill et al.(1998), the salty Slope Current water penetrated on the outer shelf near the surface (Hill, 1995) introducing a horizontal salinity gradient at shallow depths. Then winter cooling reduced slightly the temperature of the more saline water on the shelf, thus making it denser than the surrounding water. Observed values at 350m depth were ΔT=-0.19°C, (note the negative value), ΔS= -0.046 PSU, $\Delta\rho$=-0.005 kg/m3, R_ρ= (0.032)/(-0.036).

As advection of salinity plays a major role, the theory based on an assumption of purely local cooling should not be applied here. However we will test the sensitivity of theory by formally applying Eqs (2) – (4) to this case, taking H_s=110m, H_c=520m (Hill et al, 1998), dT/dz = 1.7×10^{-3} (°C/m) , dS/dz=1.7×10^{-4} (PSU/m) below the seasonal thermocline (Ellett and Martin, 1986). Formal application of eqs. (2) – (4) gives ΔT=+0.6°C (note the sign), ΔS= -0.03 PSU, $\Delta\rho$=-0.12 kg/m^3. As expected there is a great discrepancy with the observed values, and the calculated density contrast is 24 times greater than the observed value.

This exercise shows that the results are sensitive to the actual pre-conditioning mechanism, and Eqs (2) – (4) can be used as a helpful method to test the hypothesis of local production of density contrasts.

C. Temperature response to winter cooling assisted by advection of temperature

Extremely dense water may form during severe winters in the central North Sea. Steered by bottom topography, it cascades towards the deepest depressions of the Skagerrak (Ljoen and Svansson, 1972). Surveys across the strait during the abnormally cold winter of 1962-63 allowed tracing of the development of cascading at this site. Having acquired sufficient density excess, vertically homogeneous North Sea water reaches the southern slope of the Skagerrak and then descends down to the bottom at 600 m. The observed density ratio at 80 m, R_ρ=(-0.46/-0.28), shows the temperature being the main driver. Theory discussed earlier in this section is obviously not applicable here as a significant contribution to forming the cascading-favourable density contrast was made by horizontal advection of temperature rather than by local atmospheric forcing.

D. Temperature response to winter cooling assisted by advection of temperature and hindered by advection of salinity

Even though ultimately driven by winter cooling, dense water cascades in arid subtropical regions can be greatly influenced by salinity and particularly by horizontal salinity gradients. Cooper and Vaux (1949) were probably the first who pointed to the northern shelves of the Mediterranean Sea as favourable reservoirs for dense water formation due to winter cooling. Now the Adriatic Sea is a recognised source of dense bottom water for the eastern Mediterranean Sea (Zoccolotti and Salusti, 1987). Cold source water forms under the influence of north-east winter winds (Bora) on the northern Adriatic shoals, then it moves southwards along the shelf break and gradually deepens. When the shelf water crosses a submarine canyon at the shelf break off Cape Bari it continues to descend despite being adjacent to saltier Levantine waters. This occurs owing to a prevailing density excess due to cold temperature in the source waters. Since the most active production of dense shelf water

happens in winter, the most intensive cascading is assumed to occur in late winter and spring, or even in summer (Bignami et al., 1990).

2.2. Salinity driven cascades

Salinity enables a density contrast favourable for cascading in two ways. First, through summer heating and evaporation, a process more typical of warm climate zones. Second, through winter cooling and ice formation in the polar and sub-polar regions.

Equation (4) for the density contrast is also valid for convective deepening driven by summer evaporation and salinisation. However, summer salinisation due to evaporation is inevitably accompanied by warming of water. At temperatures far from freezing point, the increase in density due to salinity is often overcompensated by decrease due to temperature. However, density contrasts can be intensified by differences in the pattern of horizontal advection. Equation (4) and its derivatives are suitable for estimates of cascade pre-conditioning in areas with a smooth, nearly linear pycnocline, such as mid-latitude ocean margins and tropical arid zones, where convection is driven by winter cooling and summer evaporation respectively.

In ice-covered seas the physical mechanism producing the density contrast is different from ice-free seas and is schematically outlined below. If the ice cover is persistent all year round, the temperature of surface water is nearly constant and close to the freezing point. Heat fluxes from the ocean to the atmosphere do not result in any further cooling of water. Contributions of temperature to horizontal density variations in the surface layer are very small, first due to small temperature variability, and second due to low values of the thermal expansion coefficient at these temperatures. However, heat fluxes result in new ice formation and

release of brine into the water, since the salinity of new ice is only about 1/3 of the sea-water salinity.

The depth of convection is limited by a strong halocline in deep waters and by the seabed in shallow areas. The amount of brine released from the growing ice is too small to further deepen the homogeneous layer, and the thickness of the mixed layer does not change with time. Under similar meteorological conditions, ejected salt results in a greater increase of density within a shallow (H_s) layer over the shelf than within a thicker (H_c) homogeneous layer over the deep water. Thus thermal forcing from the atmosphere leads to a salinity-driven density contrast.

Another reason why a horizontal salinity gradient is formed in the surface layer of a polar sea is the difference in the rate of brine release, related to new ice formation. In particular, fast ice formation is associated with "polynyas", which are large persistent regions of open water and thin ice confined within a much thicker sea ice pack (Zakharov, 1996; Smith et al., 1990).

The equation for the density contrast induced by freezing is obtained as follows. The mass of salt per unit area, which is ejected into the water column as a result of freezing is (Martin and Cavalieri, 1989):

$$M = \rho_i h_i (S - S_i) = 0.69 \rho_i h_i S \qquad (5)$$

where S is salinity of sea water ; S_i is salinity of ice, $S_i=0.31 \cdot S$; ρ_i, h_i are density and thickness of ice, respectively, $\rho_i=0.92\ 10^3 kg/m^3$. The corresponding increase in salinity and density is

$$\Delta S = \frac{M}{\rho H}, \qquad \Delta\rho = \beta \Delta S \tag{6}$$

where ρ, H are the density and thickness of the mixed layer respectively. The additional density contrast due to freezing is

$$\Delta S_f = S_c - S_s = -0.62 S \frac{h_{is}}{H_s}\left(1 - \frac{h_{ic}}{h_{is}} \frac{H_s}{H_c}\right) \tag{7}$$

$$\Delta\rho_f = \beta \Delta S_f \tag{8}$$

where h_{is}, h_{ic} are the (cumulative) values of ice thickness formed over the shelf and deep water over a fixed period of time. If the amount of ice production is the same in shelf and deep waters, $h_{ic}=h_{is}$ and the density difference is controlled by the relative depth of the shelf (H_s) and the halocline (H_c).

Examples of different pre-conditioning mechanisms involving local salinisation are given below.

A. Salinity response to summer evaporation assisted by temperature response to winter cooling

Salinity enhancement was observed in the Spencer Gulf, which is an isolated shallow water inlet in the south coast of Australia. The net annual water loss due to evaporation is 1.25m (Bowers and Lennon, 1987), which is compensated by surface inflow of fresher water from the open sea resulting in formation of a sharp salinity front. Salinity at the head of the gulf reaches a maximum (about 50 PSU) at the end of summer. However, it does not result in cascading since its salinity excess is compensated by very high temperature. A longitudinal density gradient favourable for cascading is reached only in autumn and winter when the brine is cooled. Then the density contrast becomes very high, 0.8-1.0 kg/m^3 at 70 m depth, see Fig. 7. The density ratio reveals a predominant role of salinity, R_ρ= (-0.23)/(-0.54).

B. Salinity response to summer evaporation impeded by advection of temperature

In the tropics, salinity excess caused by intense evaporation can act as the major driving force for cascading. A good example is cascading off Banc d'Arguin, which is a shallow (less than 10 m depth) inshore bay between Cape Blanc and Cape Timiris off the north Mauritanian coast (Mittelstaedt, 1991). A specific feature of the Banc d'Arguin cascade is that in late winter, the bank is for most of the time isolated from cool offshore water by a sharp upwelling front (Peters, 1976). Strong evaporation increases the salinity over the bank, eventually overriding the temperature increase and thus making it denser than the upwelled waters offshore. In the shallowest part of the Bank isopycnals and isohalines intersect the surface, showing the apparent source of the dense, salty water (Fig. 8). The density ratio at 30 m depth, R_ρ=(0.13)/(-0.31) shows that cascading was driven by salinity against horizontal temperature gradients.

C. Salinity response to winter cooling (ice-covered seas)

The shallow Chukchi Sea with mean depth 71 m (Dobrovolsky and Zalogin, 1982) cools in winter nearly uniformly down to the freezing point. Cold and highly saline (33.7-34 PSU) water was repeatedly observed in the bottom layer of Barrow Canyon (Garrison and Becker, 1976), the sloping channel connecting the east Chukchi Sea shelf with the deep Beaufort Sea (Fig. 9). High values of salinity are attributed to the persistence of polynya in this region, exposing shelf waters to freezing winds (Winsor and Bjork, 2000). The section in Fig.10 demonstrates that the increase of density due to brine formation is sufficient for the dense plume to descend down to 70 m depth, i.e. it penetrates through the winter halocline at 50 m depth. Weingartner et al. (1998) argued that the source water at this site is sufficiently dense to submerge beneath the upper halocline in the Canadian Basin of the Arctic Ocean. Winsor and Chapman (2002) point towards the eddy transport as being the likely process for moving the dense polynya-derived waters further across the shelf.

The observed salinity contrast at 20m depth is ΔS= 31.80-34.03=-2.2 PSU. The density contrast, $\Delta\rho$ =-1.86 kg/m^3, is large compared to mid-latitudes, while the density ratio $R\rho$ = (-0.002)/(-1.85) shows that salinity is a sole driver for this cascade. Eqs. (4-a,b) give the predicted parameters of cascading, ΔS= -2.76 PSU, $\Delta\rho$= -2.23 kg m^3, where the following input data were used: ΔT=0, $h_{is}=h_{ic}$=4.8m, $S_s=S_c$=31.40 PSU before freezing (Winsor and Bjork, 2000), H_s=20m, H_c=50m. Good agreement between observed and calculated values is in favour of a predominant "brine-release" mechanism for cascading.

However, shelf water salinisation in polynyas does not always lead to dense water cascades. For instance, massive fresh water discharge to the shelf areas between Novosibirskiye Isles and Bering Strait makes these vast shelves unsuitable for dense water production.

2.3. Combined temperature-salinity driven cascades (seasonally ice-covered seas)

In those polar and sub-polar seas that are covered with ice only part of the year, cascades are often driven by a sequence of thermal and salinity responses to the atmospheric forcing. Autumn cooling brings the water column over the shelf to the freezing point, while the temperature of the upper mixed layer in the deep water is still above freezing. However, the resulting temperature contrast is insufficient for initiation of cascading due to strong summer freshening caused by seasonal ice melting over the shelf.

Further heat loss leads to additional cooling and deepening of the convective layer in the deep water, while over the shelf the same heat flux results in the ice formation. Subsequent brine ejection provides a salinity increase over the shelf in accordance with equation (6) and forms a horizontal density gradient between the shelf and the deep waters. Since the temperature of the mixed layer over the shelf is lower than that in the deep water, additional salinization required for cascading may be rather small. As a result, the temperature may appear as a sole driver of cascading, while the decisive salinity contribution may be hidden.

This mechanism has been observed in some parts of the Arctic Ocean, e.g. in the Barents Sea. Although this is entirely a shelf sea, its depth is non-uniform and ranges from 50-80 m over shoals to more than 300 m in troughs (Dobrovolsky and Zalogin, 1982); it is covered with ice only part of the year. In winter, the heat flux from the sea to the atmosphere in ice-free areas

can be as large as 500 W m^{-2} (Hakkinen and Cavalieri, 1989); more than 10 metres of ice freezes in the Western Novaya Zemlya polynya during an average winter (Winsor and Bjork, 2000).

Formation of a cascading-favourable density contrast can be seen in Fig 12, which shows changes in vertical profiles of temperature, salinity and density in early winter across the shelf and slope west off Novaya Zemlya. Four stations shown in Fig 11 were occupied twice, on 25 December 1987 and 8 January 1988 by the Russian research vessel Otto Smidt. By early winter, the seasonal pycnocline was completely destroyed by thermal convection and the convective layer reached the bottom at 40 m over the shelf, and 150m depth over the slope. By the end of December, shelf water reached its freezing point at -1.89 ^{0}C (station 1) while the slope water had temperature 1.68 ^{0}C, well above freezing (station 5). However, slope water was saltier and denser than water over the bank (Fig 12), thus forming a barrier for a shelf water cascade. On the shelf, further heat loss resulted in ice formation and increase of depth-average salinity by as much as 0.32 PSU. Analysis of σ_θ,T,S, cross-sections in Fig.13 reveals that any contribution from lateral advection was small. Over the slope, the same heat loss did not change average salinity and resulted only in a modest drop in temperature of 0.46^{0}C. By mid-January, the density contrasts between the slope and shelf inverted from a barring $\Delta\rho$ = -0.2 kg m^3 to $\Delta\rho$ = 0.05kg m^3 at 40 m in favour of the cascade. The density ratio R_ρ = (-0.17)/(0.13) shows a greater contribution of temperature, however it was salinisation of shelf waters that triggered cascading.

3. DOWN-SLOPE PROPAGATION

3.1 Physical process

To start descending down–slope, the source water has to reach the shelf break first. The delay between formation and cascading of dense water can be relatively long due to slow dense-plume propagation over a slightly inclined or flat bottom (Shapiro and Hill, 1997). On the way, dense water could partially lose its density excess, subsequently causing weaker cascading.

If frictional forces are negligibly small, then in steady-state conditions the body of dense water is in geostrophic balance and it flows horizontally along density fronts in accord with Margules equation (Gill, 1982). On a sloping bottom, a dense water plume will move along the slope following the contours of constant depth (Nof, 1983). If the dense plume is originally not in geostrophic balance, then geostrophic adjustment may cause cross-slope propagation of the plume. The spatial scale of the cross-slope displacement is constrained by the internal Rossby radius, while the time scale for the adjustment is of the order of a pendulum day, $2\pi/f$ (Gill, 1982). Since the pre-conditioning appears to be a much slower process than the geostrophic adjustment, the dense water pool will be in a quasi-geostrophic balance most of the time.

Large-scale dense-water outflows, e.g. in the Weddell Sea or through Denmark Strait, are predominantly in geostrophic balance, and the relative contribution of frictional forces is relatively small. Shelf-edge cascades are expected to be dynamically akin to these large-scale dense water outflows; however, the important difference is a larger contribution from bottom friction to the force balance.

Transport parameters of dense water cascades are often estimated by a stream-tube numerical model (Smith, 1975), which has shown the crucial role of ambient stratification in propagation of the outflow. On the other hand, the model results were remarkably insensitive to variations of the source water density, due to damping of density contrasts by associated changes in the entrainment rate. In the framework of this model, the overflow is considered as an entirely mixed bottom-trapped gravitational current, entraining ambient water en route while moving along isobaths and gradually sinking as a whole. The eventual depth of the large-scale outflows primarily depends on the entrainment rate, which is in turn determined by several parameters, including internal Froude number. Entrainment can only reduce the density contrast, thus decreasing the buoyancy forcing, the pace of the flow and the final depth (Price and Baringer, 1994). Bottom stress affects the long-term evolution of the flow, causing its gradual descent and broadening.

The stream-tube model assumes that frictional drag is distributed uniformly across the depth of the plume. Recent numerical and laboratory experiments do not support this assumption. Shapiro and Hill (1997) used a simplified 2-layer model to examine the behaviour of dense water on sloping bottom topography and showed that the original water plume evolves into a complex three-dimensional structure. Similar results were obtained by Jiang and Garwood (1998) who used a primitive equation model. Laboratory experiments (Whitehead et al., 1990, Shapiro and Zatsepin, 1997) showed that downslope drainage of dense water is mainly confined in a thin bottom layer.

3.2 Theory

A. Initiation of cascading due to instability of temperature-salinity distribution

In an appendix we consider a bottom boundary layer under a cross-slope density gradient ρ' assuming: no along-slope gradients; no lateral diffusion; steady state; negligible cross-slope advection of momentum in the boundary layer. Writing the lateral density gradient as $d\rho/L$ over a slope S, a condition

$$R_H = \frac{d\rho \cdot S \cdot g}{\rho \cdot L \cdot f^2} < 1 \qquad (9)$$

is found for existence of a bottom boundary layer under these conditions. Hence breakdown of this boundary layer solution (when $R_H > 1$) is encouraged a large density gradient ρ' or $d\rho/L$ (up-slope being denser), steep slope S and weak rotation f. By "breakdown" we mean that there is no steady solution. The association with strong forcing by ρ' and S together with the weak rotational constraint suggests an accelerating down-slope flow. However, this has still to be tested by a time-dependent analysis and/or model experiments, which are beyond the scope of this paper.

We regard this analysis as setting favourable conditions ($R_H > 1$) for initiating cascading as an accelerating "event" rather than as steady bottom boundary layer Ekman flow. If (9) is satisfied the density gradient is not strong enough to trigger cascading. In a few confirmed cases of cascading, correlated with the developed phase of cascading (at about the time of observation), the value of R_H is near or above 1, suggesting the possibility of accelerating

down-slope flow. In most cases R_H is very small, which we interpret as consistent with the steady Ekman-layer form of cascading.

B. Down-slope transport

Analysis of observational data, modelling results and numerical experiments show that there are several regimes of down-slope propagation of dense water over sloping sea-beds. These regimes are quantitatively defined via relationships between the rate of source water production per unit length (P) and down-slope transport in the Ekman layer (Shapiro and Zatsepin, 1997; Baines and Condie, 1998). Condie (1995) introduced a quantitative parameter, *Co*, to separate various regimes:

$$Co = \frac{\sqrt{2} \cdot P}{V_{Nof} H_E} \qquad (10)$$

where $V_{Nof} = \frac{g's}{f}$ is the Nof speed, i.e. the speed with which the dense water plume would have propagated along the contours of constant depth if there had been no friction (Nof, 1983); g' is the reduced gravity acceleration; $H_E = (2\nu / f)^{1/2}$ is the Ekman depth (here notation is different from the original paper by Condie (1995)).

An intense source (*Co*>>1) will create a thick broad plume, with evolution mostly governed by geostrophy and mixing (Condie, 1995). Such a situation fits well with the large scale overflows from marginal seas, e.g. Weddell Sea (Foster and Carmack, 1976). Alternatively,

dense water can propagate down-slope due to baroclinic instability of an along slope current (Gill, 1982). Formation of spiral waves, meanders and eddies, with horizontal scale of the order of the internal Rossby radius, has been reproduced in laboratory experiments (Whitehead et al., 1990; Condie, 1995; Shapiro and Zatsepin, 1997; Lane-Serff and Baines, 1998) and numerical simulations (Chapman and Gawarkiewicz, 1995; Jiang and Garwood, 1996). In the present paper we do not discuss the formation of eddy-like structures. For a moderate source ($Co \geq 1$) the geostrophic balance may apply partly - to a level where Ekman transport equalises discharge per unit length of slope. A weak source, $Co<1$, will initiate only transport within the Ekman boundary layer.

If the thickness of the original dense water plume exceeds approximately two Ekman depths, then a stretched down-slope frontal nose is formed due to differential drag (Shapiro and Hill, 1997). Frictional forces are relatively stronger in a thin nose of dense water than in a thicker base of the cascading plume. This mechanism produces sophisticated 3D shapes of the plume and results in eventual drainage of the dense water down-slope within the layer of about two Ekman depths' thickness. In a 2D case (no variation along the shelf break), the speed, V_{down}, of down-slope density-front propagation in a fully-developed steady-state water cascade is given by Shapiro and Hill, (1997, eq (22))

$$V_{down} = 0.2V_{Nof} = 0.2\frac{g'S}{f} \qquad (11)$$

The corresponding thickness of the drainage layer is $1.8H_E$, so the maximum down slope flux, F_d, per unit length of slope is:

$$F_d = 0.36 V_{Nof} H_E \qquad (12)$$

Equation (12) is consistent with the laboratory results by Condie (1995). The critical value of the parameter Co can be obtained by equating the rate of production of dense water, P, with the down-slope flux by Ekman drainage, F_d, which gives Co_{cr} =0.5.

C. Development of temperature contrast at the transitional stage

The pre-conditioning and active stages of cascading may well overlap, if processes contributing to the increase of the density contrast between shallow and deep waters continue to act after cascading has commenced. Consider the evolution of density contrast in a simplified case where cascading is driven entirely by temperature changes due to local sea-air interaction. A heat balance over the area of the shelf, A, where dense water is formed, is made between the outgoing flux into the atmosphere and the incoming flux of warmer water, which replaces the volume of cold water drained away due to cascading (Fig.14):

$$c_p \rho A H_s \frac{dT_s}{dt} = -QA + c_p \rho L F_d \Delta T \qquad (13)$$

where H_s is the depth of the shelf, L is the length of the shelf break, over which cascading is taking place, c_p is the heat capacity of water per unit mass, Q is loss of heat to the air per unit area per unit time, $\Delta T = T_c - T_s$ is the temperature contrast between the warmer slope and colder shelf waters. From equations (11) and (12) it follows that the cascading flux F_d is a function of ΔT, which results in a non-linear equation for the temperature changes of the shelf waters

$$\frac{dT_s}{dt} = -\frac{Q}{c_p \rho H_s} + \frac{0.36 L H_E g S \alpha (T_c - T_s)^2}{f \rho A H_s} \qquad (14)$$

where S is the slope of the seabed on the ocean side of the shelf break.

Due to continuous cooling, the temperature difference increases in time, and equilibrium is reached when the supply of thermal energy by replacement water compensates the loss of energy to the atmosphere. The equilibrium temperature difference is

$$(T_c - T_s)_{eq} = \sqrt{\frac{QfA}{0.36 L c_p H_E g S \alpha}} \qquad (15)$$

and the evolution time scale is

$$\tau_{evol} = \frac{c_p \rho H_s (T_c - T_s)_{eq}}{Q} = 1.7 H_s \rho \sqrt{\frac{c_p fA}{LQH_E g S \alpha}} \qquad (16)$$

In cases where the change in temperature of slope water is negligibly small, and the initial temperature contrast is zero, equation (14) has an analytical solution

$$(T_c - T_s) = (T_c - T_s)_{eq} \cdot \mathrm{th}(\frac{t}{\tau_{evol}}) \qquad (17)$$

where *th(...)* is the hyperbolic tangent.

An alternative to (15) as an estimate of shelf-ocean temperature difference was derived from laboratory experiments by Whitehead (1993). A best fit to his laboratory experiments is given by the equation

$$(T_c - T_s) = \frac{1}{g \cdot \alpha \cdot H_s}(7.4 \cdot q^{2/3} + 0.6 \cdot f \cdot W \cdot q^{1/3}) \qquad (18),$$

where:

$$q = \frac{g \cdot \alpha \cdot Q \cdot W}{\rho \cdot c_p}$$

W=A/L is the width of the shelf; Q is the outward heat flux (here notation is different from original paper by Whitehead (1993)).

3.3 Observations

Detailed modelling work often needs a large amount of observational data as initial and boundary conditions. Available observations of cascading events provide only limited sets of hydrographic data. However in many cases, simplified process-oriented models can reveal a particular mechanism of a cascade from comparing model results against the observed data

(e.g. Hill et al, 1998). These models allow further estimates of cascading parameters that were not observed directly, e.g. time evolution of density contrasts or down-slope fluxes.

In order to check the criterion (9) for possible initiation (acceleration) of cascading, we have chosen the examples that (i) show evidence of cascading at the time of the measurements and (ii) allow an estimate of the initial density gradient. In most cases the remaining evidence gives R_H <0.1, easily satisfying the criterion for a steady boundary layer, as may be expected longer-term after any accelerating "event" and consequent reduction of the initiating density gradient.

A. Barents Sea.

The dense plume shown in Fig 15 is bordered by the density isoline σ_θ=28.1 and clearly indicates that the plume sank from the top of the seamount (depth levels about 100-150 m) down to the valley at depths 250-330m. One might hypothesise that during the previous cold season, December 1975 to April 1976, a body of dense water was formed above the plateau due to surface cooling and salinization and this water occupied the entire depth range from the surface to the top of the seamount.

The conditions for cascading can be assessed by the R_H parameter. The excess density is $d\rho$ = 0.15 kg/m^3 between the two stations separated by L = 47 km; the average slope S is 0.0019 and f = 1.4×10^{-4}s^{-1} for latitude 76°N. The parameter R_H is about 3×10^{-5}; the criterion for a steady boundary layer is easily satisfied. Hence we expect the dense down-slope flow to progress steadily rather than as an "event". This accords with the time of observation

(August) being long after any "event". However, is it really possible to observe any remnants of winter cascades half a year afterwards, at the end of summer?

Let us examine the rate of dense water overflow in removing the body of water that had been formed during the winter season. The plateau in Fig.11 has an elongated shape in plan view, so most of the dense water would sink down the side slopes shown in Fig.15. Both the western and eastern side slopes of the plateau have the same value of *S*, about 4.6×10^{-3}. The reduced gravity acceleration is g'= 1.4 mm s^{-2}, the width of the plateau at its top is L=80 km, the volume of the original dense water pool per unit length along the plateau is $L \cdot D = 10^7$ m^2, and the Nof speed is V_{Nof}= 47mm/s. The Ekman depth is estimated from the thickness of the near-bottom dense water tongue at the top of the western edge of the plateau as H_E =15m. The total down-slope flux (per unit length) on both slopes, as estimated by equation (14), is

$$F_{tot} = 2F_d = 2 \cdot 0.36 V_{Nof} H_E = 0.51 (m^2 / s),$$

and the estimated time for the entire dense water body to sink from the plateau is

$$t_{casc} = \frac{L \cdot D}{F_{tot}} = 1.8 \times 10^7 \, s \approx 7 \; (months)$$

This estimate confirms that it is quite likely that later stages of winter cascading can be observed in the following summer.

B. Rockall Bank

The second example comes from several available surveys across Rockall Bank (Figs. 3,4,5). In addition to the estimates of the time scale for dense water removal, the data from Rockall Bank allow us to calculate the temperature contrasts across the density front using alternative models and compare the results with observations.

Rockall Bank is a narrow rise extending from the south-west to the north-east. The R_H parameter is calculated using the data from the January 1967 survey: $d\rho$=0.12 (kg m^{-3}), L=25 (km), *S*=0.011, f=1.2x10^{-4}(s^{-1}). The value R_H=0.04 allows a steady bottom Ekman layer. Taking the width of the shallowest area over the bank as 50 km and the depth over the bank D as 150 m (Fig. 2), the volume of the original dense water pool per unit length along the bank is calculated as L·D=7.5x10^6 m^2. The data from the 1967 winter survey (Fig. 5) give the Nof speed as 94 mm/s. Dense water flux per unit length, calculated using formula (14), is F_d=0.51 m^2/s using H_E = 15 m. Assuming that the dense water drains outside the source area mostly down the western slope (Fig. 4) we obtain the estimate of time needed to remove all dense water from the bank:

$$t_{casc} = \frac{LD}{F_d} = 1.4 \times 10^7 \; s \approx 6 \; (months)$$

In February 1967 the initial stage of cascading was recorded. So, the remnants of winter cascading are expected to be found over the bank during the following summer. This conclusion is indirectly confirmed by two summer surveys in July 1910 and in July 1966, clearly demonstrating a notable amount of dense water over Rockall Bank.

Equation (15) gives the following equilibrium values: $\Delta T_{eq}=1.43\ ^{o}C$, $\tau_{ev}=2.8$ months, taking the heat loss as $Q=125$ Wm^{-2} (da Silva, http://cer.ori.u-tokyo.ac.jp/toolmap/OSU-map.html). As there was less than 2 months' interval between December (still at the pre-conditioning phase prior to cascading) and the survey (end of January), the equilibrium stage was not fully achieved. Equation (17) predicts the 'transitional' temperature contrast as $\Delta T = 0.88$ °C, which gives a much better match with the observed value, $\Delta T_{obs}=0.75$°C, than the equilibrium eq (15), $\Delta T_{eq}=1.43\ ^{o}C$, or the laboratory-derived estimate (18) for equilibrium, $\Delta T_{lab}=2.69$°C.

4. FATE OF CASCADING PLUMES

After initiation of cascading, the dense plume down the slope is in effect a (particular form of) gravity current. Due to entrainment and detrainment of nearby waters, the dense plume partially loses its volume, momentum and density contrast (Hill et al., 1998; Baines, 2001). Laboratory experiments show that multiple layers of mixed water can depart from the main plume (Voropaev et al., 1978). The final depth of intrusion depends crucially on the amount of ambient water that is mixed into the plume. For instance, Price and Barringer (1994) have shown that the (initially) densest of all overflows, the Mediterranean overflow water, finds its equilibrium density at mid-depth whereas the Denmark Strait overflow water remains bottom-trapped.

The density contrast will also decrease during descent if (usually) there is stable ambient stratification. However, entrainment/detrainment during the descent does not completely destroy the core of dense shelf water (Baines, 2002). Baines (2001) found that after initial

adjustment (during which substantial mixing may occur, especially on steeper slopes) typically a bottom layer of approximately constant mean thickness is reached; mixing (with turbulent entrainment) takes place in the upper part of this layer. Eventually the plume approaches its level of neutral density and leaves the sloping bottom.

4.1 ENHANCEMENT OF DEEP WATERS VENTILATION

It is believed that under similar meteorological conditions, supply of shelf waters via cascading is a more efficient way of ventilating deep and intermediate waters than convective mixing in the adjacent deep areas (Cooper and Vaux, 1949). The maximum depth of ventilation, H_v, can be estimated using equation (4) and assuming that shelf water sinks as deep as its density level allows, without any mixing with ambient water.

$$H_v - H_c = \frac{\rho_c - \rho_s}{d\rho/dz} = \frac{1}{2}\frac{(H_c - H_s)^2}{H_s} = \frac{H_s}{2}\left(\frac{H_c}{H_s} - 1\right)^2 \qquad (19)$$

where we used a linear equation for density

$$\frac{d\rho}{dz} = (\beta\frac{dS}{dz} - \alpha\frac{dT}{dz})$$

This increase in the ventilating depth can be quite substantial. In the case of the cascade from *Rockall Bank* (see sub-section 3.3), H_c=500m, H_s=150m and the maximum depth of cascade water is H_v=908m according to equation (19), which is consistent with the observed values of about 850m (Fig. 3). Close coincidence of observed and theoretical values is in favour of

insignificant mixing with ambient water. The increase in penetration depth against deep convection is as large as 850/500=1.7.

In the *Barents Sea*, the depth of free convection was H_c=150m (January 1988) and the cascaded water reached the bottom at H_b=205m, which is consistent with the theoretical estimate H_v=230m, the gain being 205/150=1.4.

The situation in the *Chukchi Sea* is similar. The predicted maximum depth of cascaded water is 73m, while in reality water reached the bottom at 80m. The calculated gain is 80/50=1.6.

Equation (19) is sensitive to the physical mechanism of pre-conditioning. For instance, its formal application to the *Malin cascade* would give an obviously unreasonable value of H_v= 1260m (at H_c=500m and H_s=110m). This discrepancy is consistent with the bad match of Eq (4) with the observed pre-conditioning parameters, and is due to the significant contribution of lateral advection as discussed in sub-section 2.1 (B).

4.2 PLUME DISPERSION

After the head of a cascading plume has reached its equilibrium density level, it detaches from the bottom, intruding into the ambient water as an isopycnal layer. Heat and salt exchange with the surrounding water causes further evolution of cascade-origin intrusions. Double-diffusion (either “finger” or “diffusive”) is expected to be the most efficient mechanism controlling this process (Turner, 1978). Strong ambient currents may additionally facilitate distant spreading of cascading water from the source area (Tomczak, 1985). Benthic

topographic irregularities are able to facilitate assimilation of the cascade-origin water. As argued by Armi (1978), in areas where isopycnal surfaces intersect the seabed, shear turbulence of bottom flow may lead to splitting of an initially uniform bottom boundary layer into step-like structures. Hence, the developed fine structure (from meters to a few tens of meters) is observed in zones where cascading water is expected to level out (Armi, 1978; Broecker and Bainbridge, 1978).

If the density excess in the descending water remains at the bottom of the slope, cascade-origin water is able to spread over the benthic ocean as the bottom water mass (e.g. Antarctic Bottom Water), preventing stagnation in sea-floor depressions. Joint CTD-hydrochemical-turbidity measurements from the Mid-Ocean Canyon (to the south-east of the Newfoundland Ridge) have shown 20-40m thick warm and salty bottom layers with decreased silica and increased oxygen content (Broecker and Bainbridge, 1978). A few hundreds miles to the west of this site, Armi (1978) reported similar intrusions at 150-200m above the bottom. Denmark Strait overflow water, propagating along the canyon axis and leaving the sea floor after entering the Sohm abyssal plain, is argued to be the source of these intrusions.

Evolution of a sediment-laden plume reveals some specific features (Backhaus et al., 1997). First, the final depth of the plume is not explicitly dependent on the thermohaline density contrast due to extra weight of suspended particles. Second, after reaching the flat area where turbulence within the plume weakens, sediment deposition may lead to considerable lightening of the intrusion, initiating its ascent.

5. DISCUSSION AND CONCLUSIONS

We have identified, by world-wide trawling of raw data bases, several different mechanisms of pre-conditioning for cascades, including

- temperature response to (winter) cooling of surface waters (in some cases modified by advection of temperature or salinity)
- salinity response to (summer) heating and evaporation of surface waters (with examples modified by subsequent winter cooling or temperature advection)
- salinity response to winter cooling of surface waters and ice formation in ice-covered seas
- combined temperature and salinity response to winter cooling in seasonally ice-covered seas.

We have also developed simple models, which allow estimates of the parameters for pre-conditioning of cascading and down-slope fluxes as well as evolution of the temperature contrasts during cascading events. We introduced a helpful criterion of initiation of cascading, which is based on stability considerations. Compliance or non-compliance of observations with these simple and easy-to- use models has been related to the stage of cascade development and to local factors, as follows. Estimates of observed down-slope transport rates in (sub-section 3.3) accord with theory (sub-section 3.2), which is thereby substantially validated.

In the majority of cases, the initiation parameter $R_H < 1$; the interpretation is that the observations are still in the pre-conditioning phase or (more usually) after any phase of accelerating down-slope flow. At the pre-conditioning stage, theoretical values of the temperature and salinity contrasts compare well with observation where dense water is

produced from local sources. Where advection plays a major role the theory becomes invalid. Formal application of theory produces unrealistic figures in such cases. The positive side however is that the models provide a tool to check that advection is a major player.

At the developed stage of cascading, the application of the simplified version of the model by Shapiro and Hill (1997) gives reasonable estimates of down-slope fluxes and life-span time scales. It was found that sometimes cascading starts before the cooling period finishes, so that the temperature contrasts continue to develop. Model estimates of temperature contrasts at this intermediate stage give a better coincidence with observations than previously published methods.

Typical values of cascading fluxes in sub-section *3.3* were $F_{tot} \sim 0.5$ m^2s^{-1}. In other cases calculation give values up to 1.6 m^2s^{-1}. These values are comparable (when and where they occur) with other main mechanisms of shelf-ocean exchange (Huthnance, 1995), for example wind-driven flows and secondary circulations / Ekman layers associated with along-slope currents, which have perhaps the closest dynamical affinity with cascading. The particular significance of cascading is in the character (dense, oxygenated, etc.) of the water exported from shelf to ocean.

Despite their intermittent nature, dense water cascades have a clear signature in the formation of major water masses in the World ocean. One example is the formation of Antarctic Bottom Water. Two of the four major Barents Sea water masses, intermediate Barents Sea Water and Barents Sea Bottom Water, are formed during the winter season. The Barents Sea Water is formed around the whole basin due to thermal convection (Steele et al., 1995) while the

Barents Sea Bottom Water is believed to be formed in patchy patterns by cascading of cold, hyper-saline water plumes from extensive local shoals (Midttun, 1985).

We hazard a very approximate global estimate of order 10^5 (km^3yr^{-1}) or average 3 Sv, based on 1 m^2s^{-1} flux for 10^7s (nearly 4 months) each year along 10^4 km global total length of shelf when cascading occurs. In fact this figure appears probably to be an underestimate. From publications, lower and upper estimates (Sv) are:

Weddell Sea: 1.5-3.6 (Muench and Gordon, 1995; Gill, 1973; Foster and Carmack, 1976);

Other Antarctic: 0.7-1.8 (our estimate based on data from Baines and Condie, 1998)

Arctic: 1.2-2.2 (Quadfasel et al., 1988 - deep layers); 0.8-1.2 (Cavalieri and Martin, 1994 - halocline), 2.5 (Aagard et al, 1981), 0.2 (Winsor and Bjork, 2000)

Other shelves: 1-1.2 including Bass Strait 0.2 (Luick et al., 1994), Sea of Okhotsk 0.5 (Alfultis and Martin, 1987), Spencer Gulf 0.05 (Bowers and Lennon, 1987), Adriatic 0.04 – 0.08 (Bignami et al., 1990; Zoccolotti and Salusti, 1987) etc.

In particular, the Arctic estimate exceeds the 0.8 Sv estimated through-flow from Bering Strait to Fram Strait (Roach et al., 1995) and is thereby important to the Arctic halocline and deep waters.

ACKNOWLEDGEMENTS

This work was co-funded by the INTAS grant 99-1600 “Dense water overflows off continental shelves (cascading)” from the European Union.

APPENDIX: initiation of cascading

We consider a bottom boundary layer under a cross-slope density gradient ρ' ($\equiv(F_Q/H)_x$ if F_Q is a measure of the heat removed from the shelf water of depth H). The following simplifications are made: no along-slope (y) gradients (u_y = v_y = 0 = p_y); no lateral diffusion; steady state; negligible cross-slope advection of momentum in the boundary layer. In co-ordinates x, z rotated through the bottom slope θ so that x is down-slope, governing 3-dimensional equations of motion (*cf*. Garrett, McCready & Rhines, 1993) are:

$$-fv = -\rho_0^{-1} p_x + \rho_0^{-1} g\rho \cdot \sin\theta + (\nu u_z)_z \qquad \text{(A.1a)}$$

$$fu = (\nu v_z)_z \qquad \text{(A.1b)}$$

$$p_z = -g\rho \cdot \cos\theta \qquad \text{(A.1c)}$$

$$u\rho_x + w\rho_z = (K\rho_z)_z \qquad \text{(A.1d)}$$

$$u_x + w_z = 0 \qquad \text{(A.1e)}$$

Boundary conditions are

$$\rho_x \to \rho' \cos\theta, \qquad \rho_z \to \rho' \sin\theta, \qquad \text{as } z \to \infty$$

$$v_z, u, w \to 0 \qquad \text{as } z \to \infty \qquad \text{(on the scale } (\nu/f)^{1/2})$$

$$u, v, w, \rho_z = 0 \qquad \text{at } z = 0$$

Here *(u, v, w)* are *(x, y, z)* components of velocity, *p* is pressure, *g* is gravitational acceleration ~ 10 m s^{-2}, ρ is a density perturbation relative to a mean density $\rho_0 \sim 10^3$ kg m^{-3}, f is the Coriolis parameter ~ 10^{-4} s^{-1}, ν is a vertical viscosity and *K* is vertical diffusivity ~ 10^{-2} $m^2 s^{-1}$. Subscripts denote differentiation.

Let $u = \psi_z$, $w = -\psi_x$. Solutions with w, ρ_{xx}, $\rho_{zx} = 0$ (justifying neglect of lateral diffusion) are

$$\rho_z = \frac{\rho_x \psi}{K} \qquad \text{and } \psi \to K_\infty \tan\theta \text{ as } z \to \infty \quad \text{(from A.1d taking } \psi = 0 \text{ on } z = 0)$$

$$\nu v_z = f(\psi - K_\infty \tan\theta) \qquad \text{(from A.1b)}$$

$$(\nu\psi_{zz})_{zz} + \psi\left(\frac{f^2}{\nu} + \frac{g\rho' \sin\theta \cdot \cos\theta}{K\rho_0}\right) = \frac{f^2 K_\infty \tan\theta}{\nu} - \frac{g\rho'}{\rho_0}\cos^2\theta \qquad \text{(A.2)}$$

[from $(A.1a)_z$ using (A.1c) and these substitutions]. Denoting the coefficient of ψ in (A.2) by G, and the right-hand side by R, the solution for constant K, ν is a combination of a particular integral R/G and a complementary function comprising decaying exponentials in z>0 (so that ψ is bounded) and summing to give $\psi = 0$ on z=0, ie. for arbitrary c

$$\psi = \frac{R}{G} \cdot [1 - c \cdot \exp(-q_1^+ z) - (1 - c) \cdot \exp(-q_2^- z)]$$

where

$$\nu(-q^\pm)^4 = -G \text{ ,i.e. if G>0 then } q_1^\pm = (G/4\nu)^{1/4}(\pm 1 + i), \qquad q_2^\pm = (G/4\nu)^{1/4}(\pm 1 - i),$$

and c is chosen so that $\psi_z = u = 0$ on z=0.

If G<0, then the complementary functions are exp(±qz), exp(±iqz) where νq^4=-G; there is only one exponentially-decaying solution. Hence there is no steady-state boundary-layer solution controlled by ν, K and satisfying ψ = 0 = u on z=0. The criterion for this breakdown of the boundary-layer solution (G<0) is, from the definition of G after (A.2) with Prandtl number $\sigma \equiv K/\nu$,

$$\rho' < -\frac{\rho_0 f^2 \sigma}{g \sin\theta \cos\theta}$$

or (for small slopes $H_x \sim \sin\theta$, $\cos\theta \sim 1$)

$$\rho' g H_x > f^2 \rho_0 \sigma$$

Writing the lateral density gradient as $d\rho/L$ over a slope s,

$$R_H = \frac{d\rho \cdot s \cdot g}{\rho \cdot L \cdot f^2} < 1 \qquad \text{(A.3)}$$

is the steady bottom boundary layer criterion.

REFERENCES

Aagaard, K., L.K. Coachman, E. Carmack, On the halocline of the Arctic Ocean, *Deep Sea Res., 28A*, 529-545, 1981.

Alfultis, M.A. and S. Martin, 1987, Satellite passive microwave studies of the Sea of Okhotsk ice cover and its relation to oceanic processes, 1978-1982, *J. Geophys. Res., 92*, 13013-13028, 1987

Armi, L., Some evidence for boundary mixing in the deep ocean, *J. Geophys. Res., 83*(C4), 1971-1979, 1978.

Backhaus, J.O., H.Fohrmann, J.Kampf and A.Rubino, Formation and export of water masses produced in Arctic shelf polynyas – process studies of oceanic convection, *ICES J. Mar. Sci., 54*, 366-382, 1997.

Baines, P.G., S. Condie, Observations and modelling of Antarctic downslope flows: a review, in *Ocean, ice, and atmosphere: interactions at the Antarctic continental margin, Antarctic Research series, 75*, 29-49, 1998.

Baines, P.G., Mixing in flows down gentle slopes into stratified environments, *J.Fluid Mech., 443*, 237-270, 2001

Baines, P.G., The hydraulics of downslope flows in rotating stratified environments, paper presented at XXVII EGS General Assembly, Nice, France, 2002.

Bignami, F., G. Mattietti, A. Rotundi, E. Salusti, On a Suigimoto-Whitehead effect in the Mediterranean Sea: sinking and mixing of a bottom current in the Bari Canyon, southern Adriatic Sea, *Deep Sea Res., 37*, 4, 657-665, 1990.

Bowers, D.G., and G.W.Lennon, Observations of stratified flow over a bottom gradient in coastal sea, *Cont. Shelf Res., 7*, 9, 1105-1121, 1987.

Broecker, W.S., and A.Barnbridge, An abyssal shear zone, *J. Geophys. Res, 83*(C4), 1963-1966, 1978

Cavalieri, D.J. and S. Martin, The contribution of Alaskan, Siberian, and Canadian coastal polynyas to the cold halocline layer of the Arctic Ocean, *J. Geophys. Res., 99*, 18343-18362, 1994.

Chapman, D.C., and G. Gawarkiewicz, Offshore transport of dense shelf water in the presence of a submarine canyon, *J. Geophys. Res., 100*(C7), 13,373-13,387, 1995.

Condie, S.A, Descent of dense water masses along continental slopes, *J. Marine Res., 53*, 897-928, 1995.

Cooper, L.N.H., and D.Vaux, Cascading over the continental slope of water from the Celtic Sea, *Journ. of the Marine Biological Association of the UK, 28*, 719-750, 1949.

Da Silva, A.M., Air-sea interaction map (http://cer.ori.u-tokyo.ac.jp/toolmap/DaSilva.html), based on: da Silva, A. M., C. C. Young, and S. Levitus, Atlas of Surface Marine Data 1994, Volume 1: Algorithms and Procedures. *NOAA Atlas NESDIS 6*, U.S. Department of Commerce, NOAA, NESDIS, 83 pp., 1994

Dade, W,B., H.E.Huppert, Predicting the geometry of channelized deep-sea turbidites, *Geology, 22,* 645-648, 1994.

Dobrovolsky, A.D., and B.S. Zalogin, Morya SSSR. Izdatelstvo Moscovscogo Universiteta, Moscow, 192 pp., 1982, (in Russian).

Ellet, D.J., A. Edwards, and R.Bowers, The hydrography of the Rockall Channel – an overview, *Proc. of Roy. Soc. of Edinburgh, 88B*, 61-81, 1986

Ellett, D.J., 1968, The cold "winter-water" of Rockall Bank, *ICES CM 1968/C:24*, 14pp, 1968.

Ezer, T., and G.L. Weatherly, A numerical study of the inreraction between a deep cold jet and the bottom boundary layer of the ocean, *J. Phys. Oceanogr., 20*, 801-816, 1990.

Foster, T.D., and E.C. Carmack, Frontal zone mixing and Antarctic bottom water formation in the Southern Weddell Sea, *Deep Sea Res., 23*, 301-317, 1976.

Garrett, C., P. MacCready, and P. Rhines, Boundary mixing and arrested Ekman layers: rotating stratified flow near a sloping boundary, *Annual Review of Fluid Mechanics, 25*, 291-323, 1993.

Garrison, G.R., and P.Becker, The Barrow submarine canyon: a drain for the Chukchi Sea, *J. Geophys. Res., 81*, 4445-4453, 1976.

Gill, A.E., Circulation and bottom water production in the Weddell Sea, *Deep-Sea Res., 20*, 111-140, 1973.

Gill, A.E, Atmospheric-Ocean Dynamics, New York, Academic Press, 662 pp., 1982.

Hakkinen, S., and D.J. Cavalieri, A study of ocean surface heat fluxes in the Greenland, Norwegian and Barents Seas, *J. Geophys. Res., 94*(C5), 6145-6157, 1989.

Hill, A.E, Leakage of barotropic slope current onto the continental shelf, *J. Phys. Oceanogr., 25*, 1617-1621, 1995.

Hill, A.E., A.J.Souza, K.Jones, J.H.Simpson, G.I.Shapiro, R.McCandliss, H.Wilson, and J.Leftly, The Malin cascade in winter 1996, *J. Mar. Res., 56*, 87-106, 1998.

Huthnance, J.M., Circulation, exchange and water masses at the ocean margin: the role of physical processes at the shelf edge, *Progr. Oceanogr., 35*, 353-431, 1995.

Huthnance, J.M., The Rockall slope current and shelf edge processes, *Proc., Roy. Soc. Edinburgh, 88B*, 239-263, 1986.

Jiang, L., and W. Garwood, Three-dimensional simulations of overflows on continental shelves, *J. Phys. Oceanogr., 26*, 1214-1233, 1996

Jiang ,L., and W. Garwood, Effects of topographic steering and ambient stratification on overflows on continental slopes: a model study, *J. Geophys. Res.*, 103(C3), 5459-5476, 1998

Jones, E.P., B.Rudels, and L.G.Anderson, Deep waters of the Arctic Ocean: origins and circulation, *Deep Sea Res., 42*, 5, 737-760, 1995.

Killworth, P.D, Mixing on the Weddell Sea continental slope, *Deep Sea Res., 24*, 427-448, 1977.

Lane-Serff, G.F., and P.G. Baines, Eddy formation by dense flows on slopes in a rotating fluid, *J. Fluid Mech., 363*, 229-252, 1998.

Lane-Serff, G, Overflows and cascades, in *Encyclopedia of Ocean Sciences*, edited by J. H. Steele, New York, Acadimic Press, 2001.

Ljoen, R., and A. Svannson, Long-term variations of subsurface temperature in Scagerrak, *Deep Sea Res., 19*, 277-288, 1972

Luick, J.L., R. Käse and M. Tomczak, On the formation and spreading of the Bass Strait cascade, *Continental Shelf Res., 14*, 385-399, 1994.

Martin, D.J., Cavalieri, Contribution of the Siberian shelf to the Arctic Ocean intermediate and deep water, *J. Geophys. Res., 94*, 12, 12,725-12,738, 1989.

Meincke, J., B.Rudels, H.Friedrich, The Arctic Ocean – Nordic Seas thermohaline system, *ICES Journ. of Mar. Sci., 54*, 283-299, 1997.

Midttun, L, Formation of dense bottom water in the Barents Sea, *Deep Sea Res., 32*, 10, 1233-1241, 1985.

Mittelsdaedt, E., The ocean boundary along the northwest African coast: circulation and oceanographic properties of the sea surface, *Progr. Oceanogr., 26*,307-355, 1991.

Muench, R.D. and A.L. Gordon, Circulation and transport of water along the western Weddell Sea margin, *J. Geophys. Res., 100*, 18503-18515, 1995.

Nansen, F., The waters of the north-eastern North Atlantic, *Int. Rev. Hydrobiol. Suppl. to Bd.4*, 139 pp., 1913.

Nof, D., The translation of isolated cold eddies on a sloping bottom, *Deep Sea Res., 30*, 2A, 171-182, 1983.

Peters, H., The spreading of water masses of the Banc d'Arguin in the upwelling area off the Northern Mauritanian coast, *"Meteor" Forshungsergebnisse (A), 18*, 78-100, 1976.

Price, J.F., M. O'Neil Baringer, Outflows and deep water production by marginal seas, *Progr. Oceanogr., 33*, 161-199, 1994.

Quadfasel, D., B. Rudels and K. Kurz, Outflow of dense water from a Svalbard fjord into the Fram Strait, *Deep-Sea Res., 35*, 1143-1150, 1988.

Roach, A.T., K. Aagaard, C.H. Pease, Salo S.A., T. Weingartner, V. Pavlov, M. Kulakov, Direct Measurements Of Transport And Water Properties Through The Bering Strait, *J. Geophys. Res.,100,* C9, 18443-18457, 1995

Rudels B., The Theta-S relations in the northern seas: Implications for the deep circulation, *Polar Research, 4*, 133-159, 1986.

Saunders, P.M., Cold outflow from the Faroe Bank Channel, *J.Phys.Oceanogr., 20*, 29-43, 1990.

Shapiro, G.I. and A.G.Zatsepin, Gravity current down a steeply inclined slope in a rotating fluid, *Ann. Geophys., 15*(3), 366-374, 1997.

Shapiro, G.I. and A.E.Hill, Dynamics of dense water cascade at the shelf edge, *J. Phys. Oceanogr., 27*, 2381-2394, 1997.

Shapiro, G.I. and A.E.Hill, The alternative density structures of cold/salt water pools on a sloping bottom: the role of friction, *J. Phys. Oceanogr., 33***,** 390-406. 2003.

Smith, P.C., A streamtube model for bottom boundary currents in the ocean, *Deep Sea Res., 22*, 853-873, 1975.

Smith, S.D., R.D. Muench and C.H. Pease, Polynyas and Leads: an Overview of physical processes and environment, *J. Geophys. Res., 95*(C6), 9461-9479, 1990.

Steele, M., J. Morrison, and T.B. Curtin, Halocline water formation in the Barents Sea, *J. Geophys. Res., 100*(C1), 881-894, 1995.

Symonds, G., R.Gardiner-Garden, Coastal density currents forced by cooling events, *Cont. Shelf Res., 14*, 2/3, 143-157, 1994.

Tomczak, M., The Bass Strait water cascade during winter 1981, *Cont. Shelf Res., 4*, 3, 255-278, 1985.

Turner, J.S, Double-diffusive intrusions into a density gradient, *J. Geophys. Res*, 83, 2887-2901, 1978.

Turrell, W. R.; Slesser, G.; Adams, R. D.; Payne, R., Gillibrand, P. A, Decadal variability in the composition of Faroe Shetland Channel bottom water, *Deep Sea Res., Part 1; 46*; 1, 1-26, 1999.

Voropaev, S.I., A.G. Zatsepin, A.M. Pavlov, K.N. Fedorov, Laboratory experiments of structure-forming processes in a strongly stratified fluid, in *Studies of variability of physical processes in the ocean*, edited by K.N.Fedorov, Academy of Sciences of the USSR, P.P.Shirshov Institute of Oceanology. Moscow, 112-121, 1978.

Weingartner, T., D., J. Cavalieri, K. Aagaard, and Y. Sasaki, Circulation, dense water formation and outflow on the northeast Chukchi shelf, *J. Geophys. Res., 103*(C4), 7647-7661, 1998.

Whitehead, J.A., A laboratory model of cooling over the continental shelf, *J. Phys. Oceanogr. 23*, 2412-2427, 1993.

Whitehead, J.A., M. Stern, G.R. Flierl, and B.A.Klinger, Experimental observations of baroclinic eddies on a sloping bottom, *J. Geophys. Res, 95*(C6), 9585-9610, 1990.

Whitehead, J.A., Dense water off continents, *Nature, 327*, 656,1987.

Winsor, P. and G. Bjork, Polynya activity in the Arctic Ocean from 1958 to 1997, *J. Geophys. Res., 105*(C4), 8789-8803, 2000.

Winsor, P., D.C. Chapman, Distribution and interannual variability of dense water production from coastal polynyas on the Chukchi Shelf, *J.Geophys. Res. 107*, C7: art. no. 3079, 2002

Yoder, J., T.Ishimaru, Phytoplankton advection off the southeastern United States continental shelf, *Cont. Shelf Res., 9*, 6, 547-553, 1989.

Zakharov, V.F, Sea Ice in the Climate System, (in Russian), St.Petersburg, Hydrometeoizdat, 213 pp., 1996.

Zoccolotti, L., and E.Salusti, Observations of vein of very dense water in the southern Adriatic Sea, *Cont. Shelf Res., 7*, 6, 535-551, 1987.

FIGURE CAUPTIONS

Fig.1 Scheme of formation of horizontal density contrast between shelf and slope waters under identical outward heat flux. Subscripts "o", "s", "c" denote the initial state, shelf water and slope water respectively.

Fig.2. Location of transects and the bottom topography over the northwest European shelf-slope area.

Fig.3. Potential density (solid lines) and temperature (shaded areas) cross sections near the Rockall Bank in July 1910.

Fig.4. Potential density (solid lines) and temperature (shaded areas) cross sections near the Rockall Bank in July 1966.

Fig.5. Potential density (solid lines) and temperature (shaded areas) cross sections near the Rockall Bank in January 1967.

Fig. 6. Potential density (solid lines) and salinity (shaded areas) across the edge of the Malin shelf in February 1996.

Fig. 7. Potential density (solid lines) and salinity (shaded areas) along the axis of the Spencer Gulf in July 1985.

Fig. 8 Potential density (solid lines) and salinity (shaded areas) off the Banc d'Arguin in February 1972.

Fig. 9. Location of transects and the bottom topography over the eastern Chukchi Sea. Dashed line shows the boundary of coastal polynya (box 22, according to the specification introduced Winsor and Bjork (2000))

Fig. 10. Potential density (solid lines) and salinity (shaded areas) over the eastern Chukchi Sea shelf in March 1981.

Fig. 11. Location of transects and the bottom topography over the eastern Barents Sea.

Fig. 12. Vertical profiles of temperature (a), salinity (b) and potential density (c) for pairs of stations in the eastern Barents Sea, shown in Fig. 11 (triangles).

Fig. 13 (a) Potential density (solid lines) against temperature (shaded areas) on January 8 at the section shown by triangles in Fig,11; (b) Salinity (solid lines) against temperature (shaded areas) on January 8 at the section shown by triangles in Fig.11.

Fig. 14. Schematic development of temperature contrast in the transitional phase of cascading

Fig. 15. Potential density (solid lines) against temperature (shaded areas) in August 1976 at the section shown by circles in Fig,11.

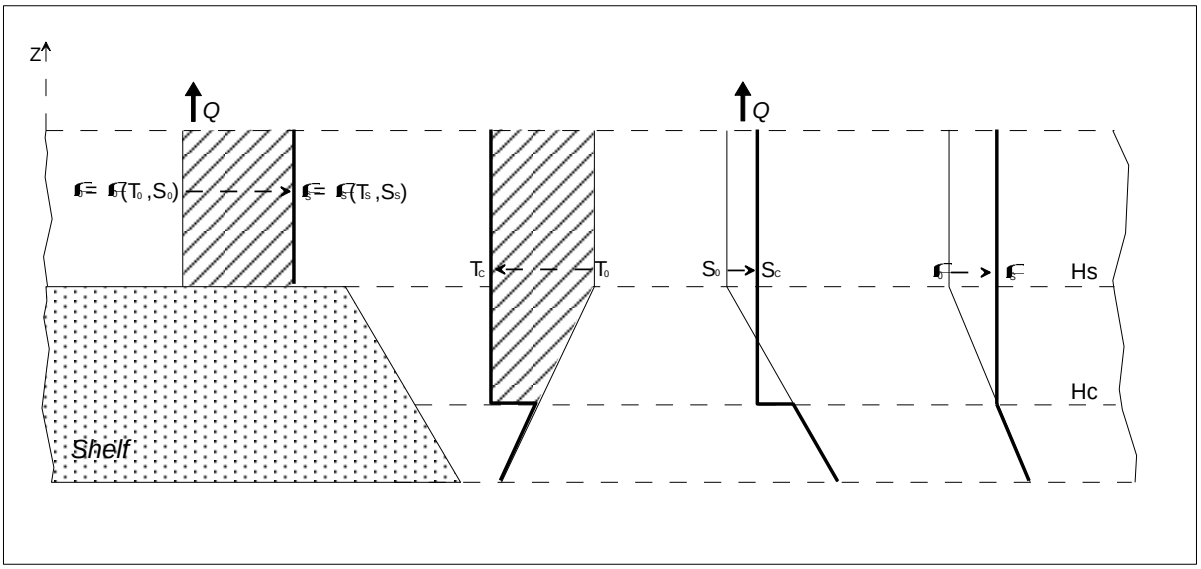

Fig.1

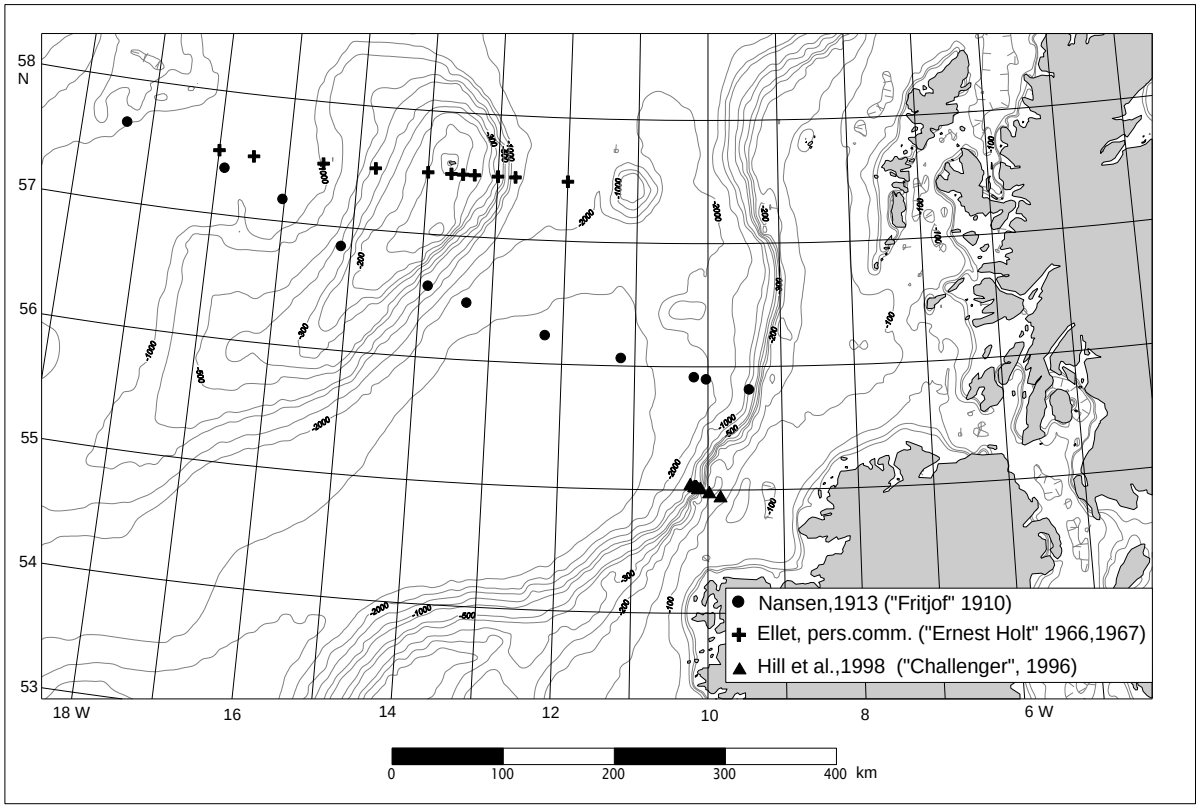
58 N
57
56
55
54
53
18 W
16
14
12
10
8
6 W
Nansen,1913 ("Fritjof" 1910)
Ellet, pers.comm. ("Ernest Holt" 1966,1967)
Hill et al.,1998 ("Challenger", 1996)
0
100
200
300
400 km

Fig.2

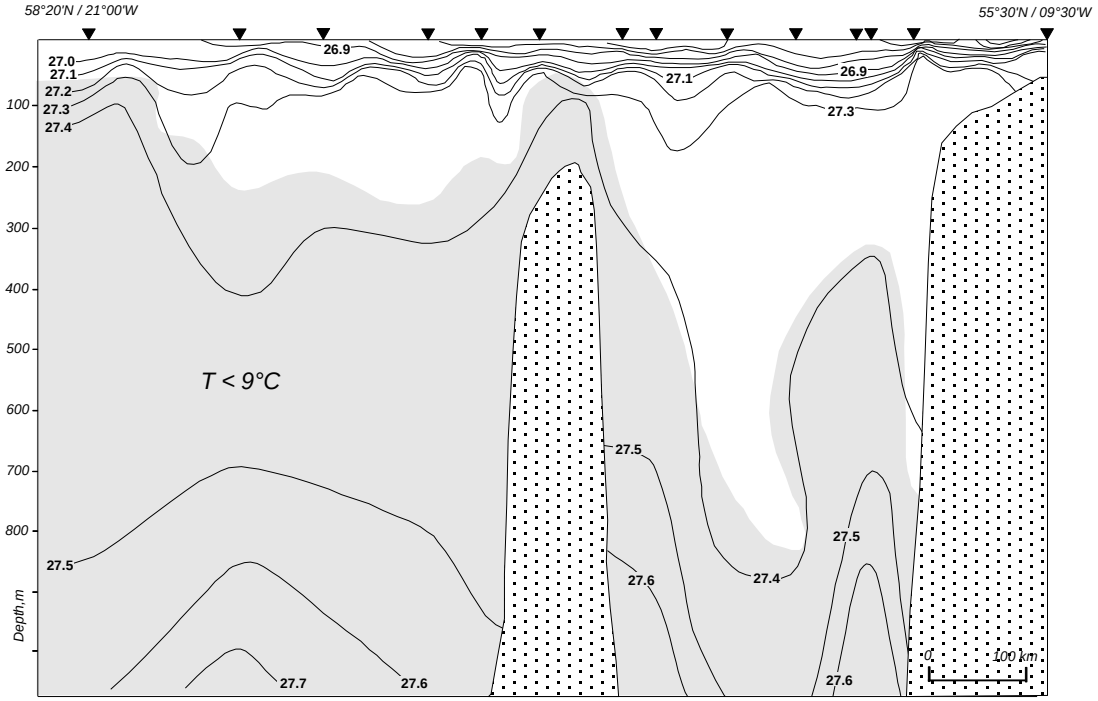
58°20'N / 21°00'W
55°30'N / 09°30'W
26.9
27.0
27.1
27.2
27.3
27.4
27.1
26.9
27.3
100
200
300
400
500
600
700
800
Depth,m
T < 9°C
27.5
27.5
27.6
27.4
27.5
27.7
27.6
27.6
0
100 km

Fig.3

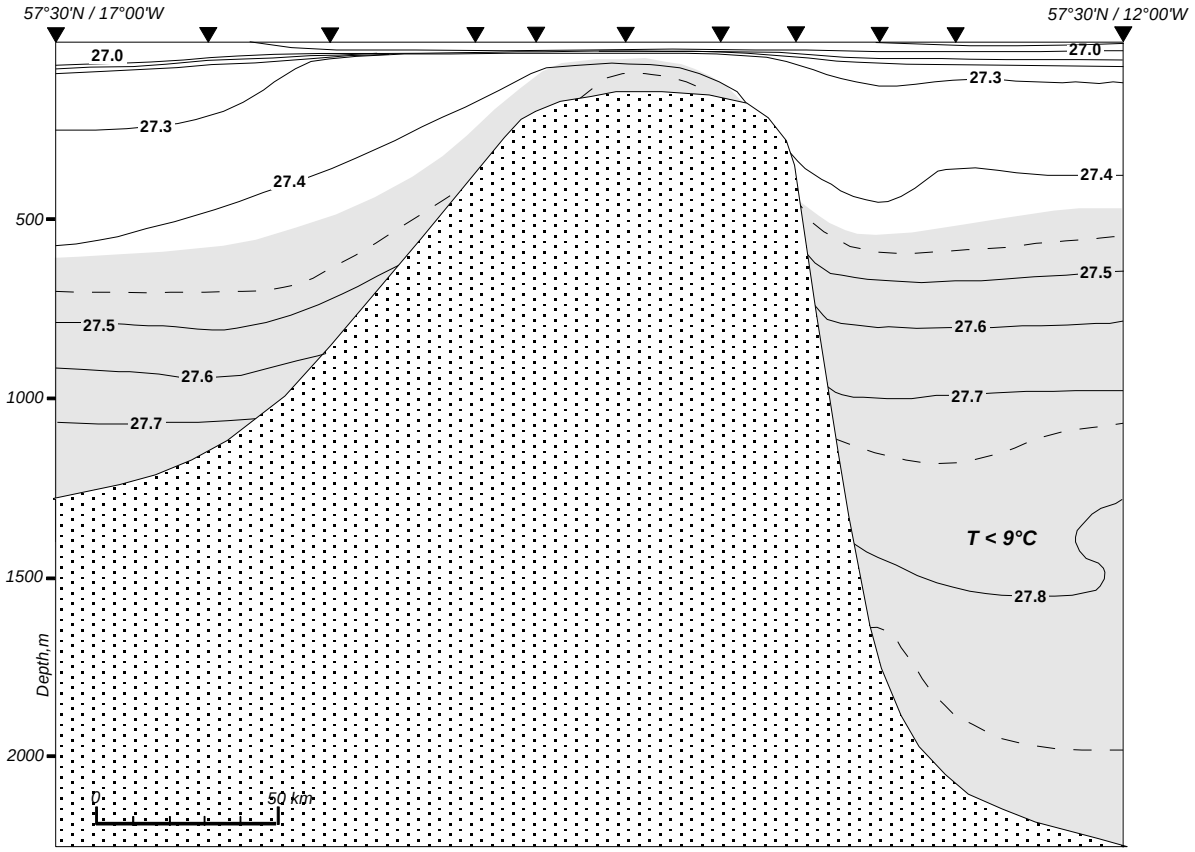
57°30'N / 17°00'W
57°30'N / 12°00'W
27.0
27.3
27.4
27.5
27.6
27.7
27.8
T < 9°C
500
1000
1500
2000
Depth,m
0
50 km

Fig.4

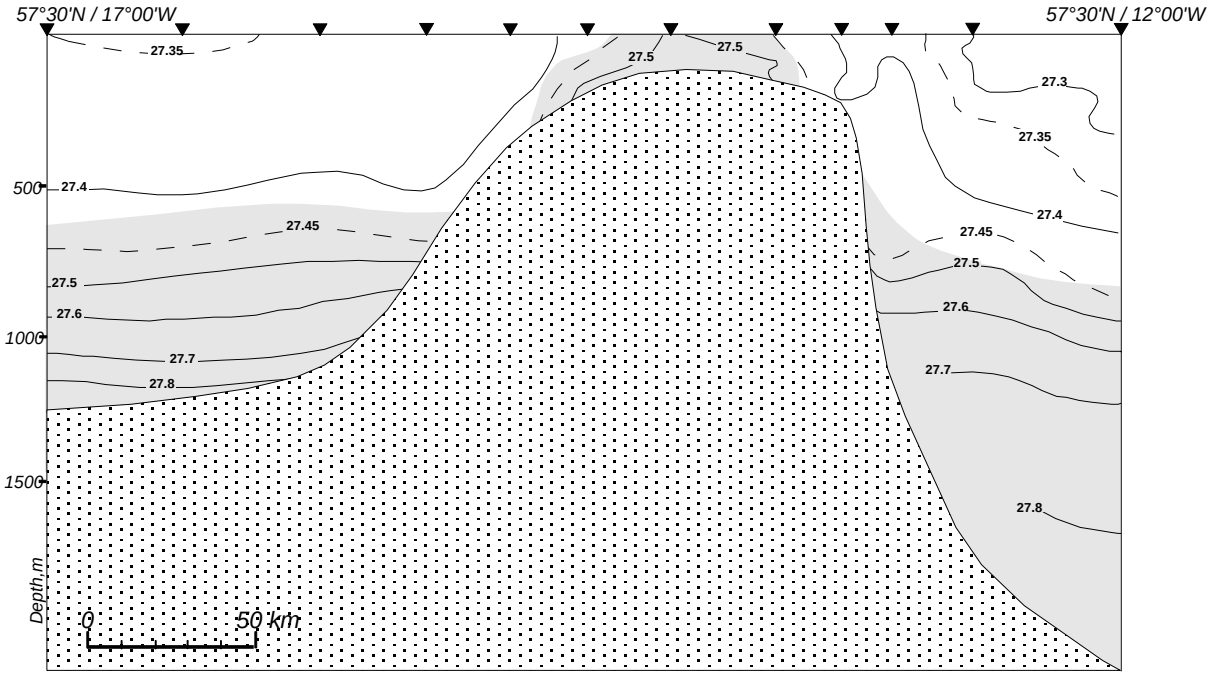
57°30'N / 17°00'W
57°30'N / 12°00'W
27.35
27.5
27.5
27.3
27.35
500
27.4
27.4
27.45
27.45
27.5
27.5
27.6
27.6
1000
27.7
27.7
27.8
1500
27.8
Depth,m
0
50 km

Fig.5

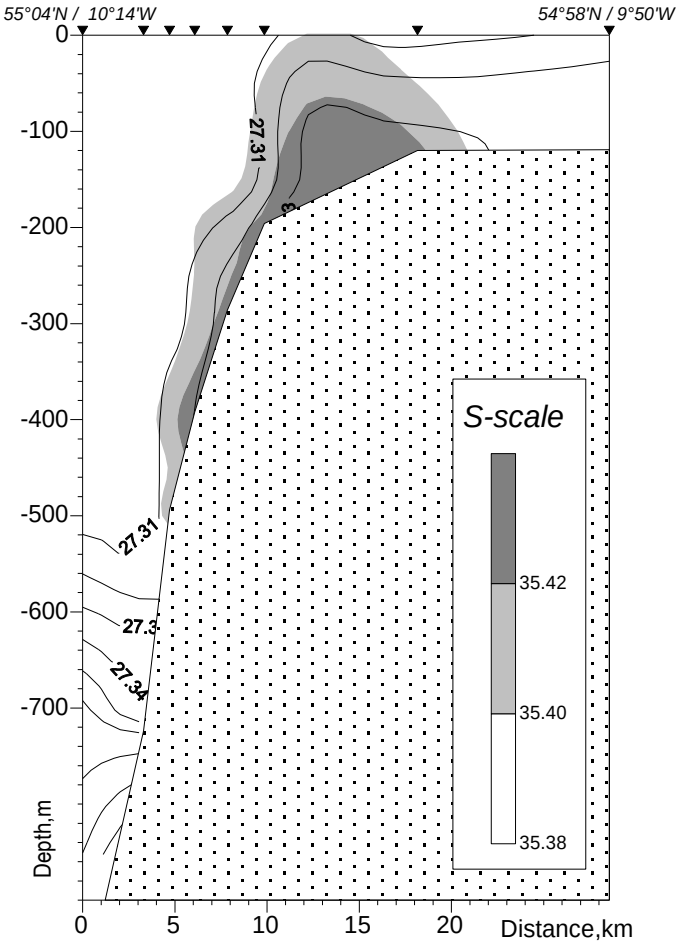
55°04'N / 10°14'W
54°58'N / 9°50'W
0
-100
-200
-300
-400
-500
-600
-700
27.31
27.31
27.3
27.34
S-scale
35.42
35.40
35.38
Depth,m
0
5
10
15
20
Distance,km

Fig. 6

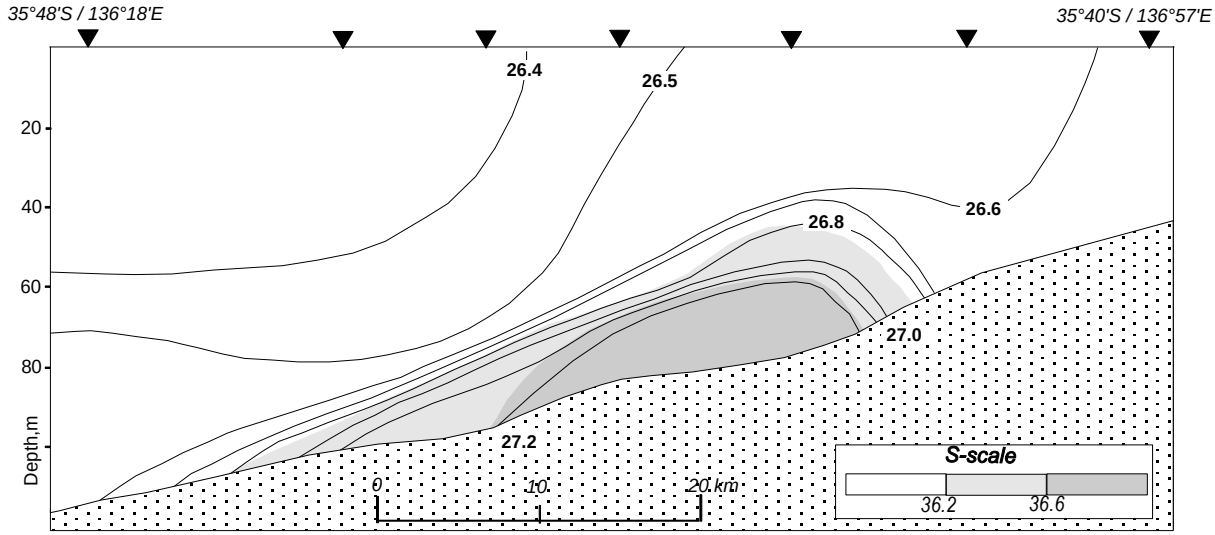
35°48'S / 136°18'E
35°40'S / 136°57'E
26.4
26.5
26.6
26.8
27.0
27.2
20
40
60
80
Depth,m
0
10
20 km
S-scale
36.2
36.6

Fig. 7

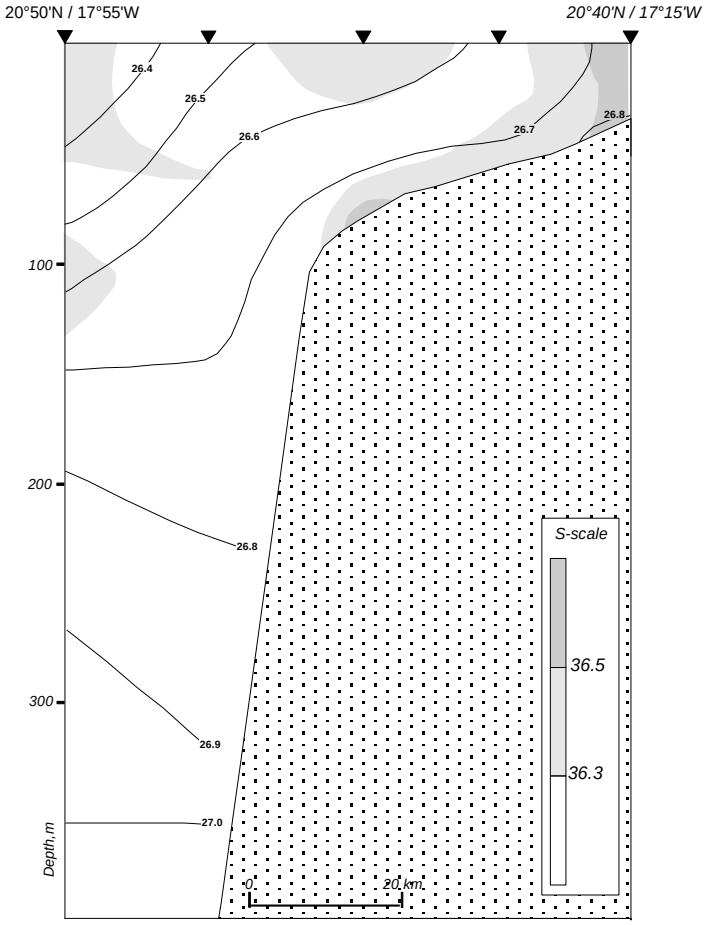
20°50'N / 17°55'W
20°40'N / 17°15'W
26.4
26.5
26.6
26.7
26.8
100
200
26.8
300
26.9
27.0
Depth, m
S-scale
36.5
36.3
0.
20 km.

Fig.8

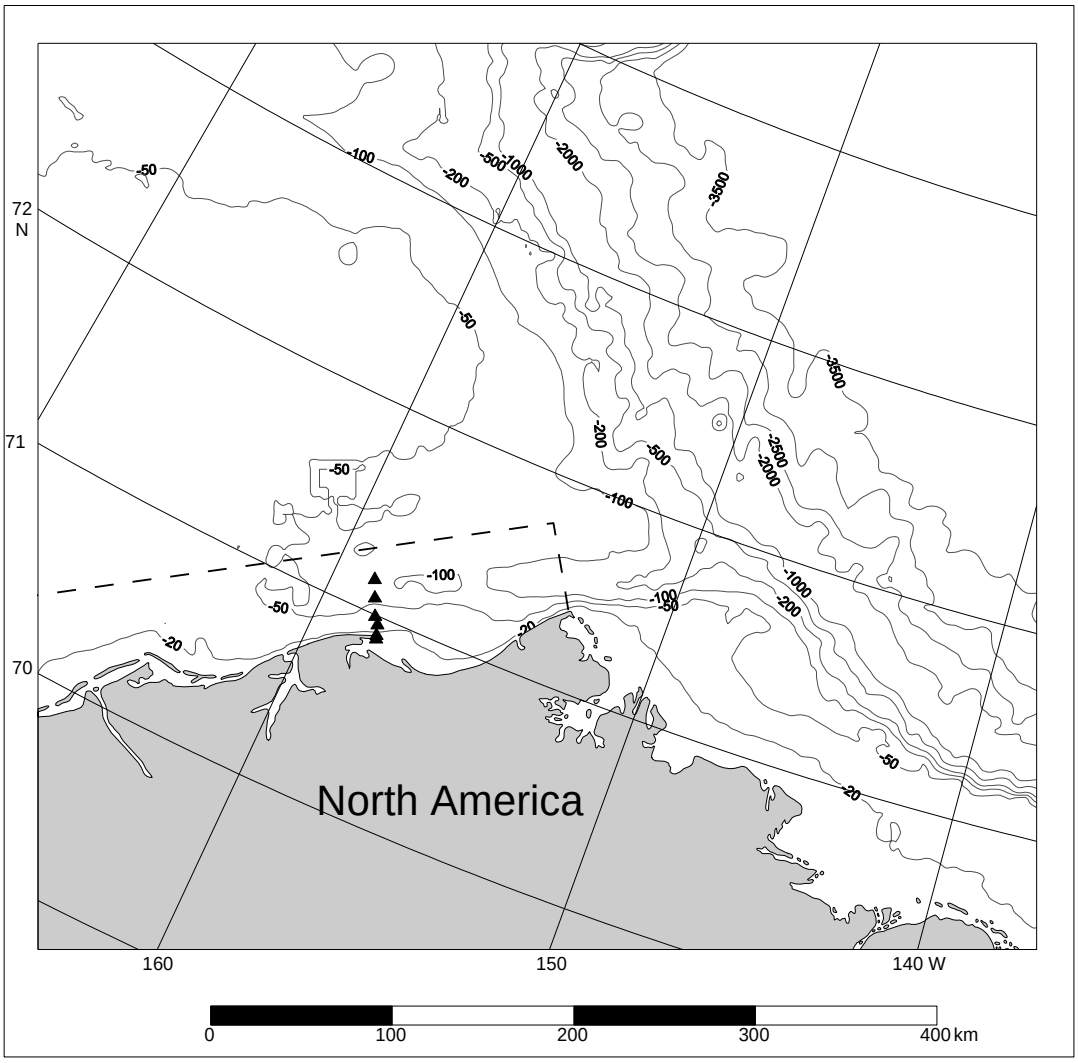

Fig. 9

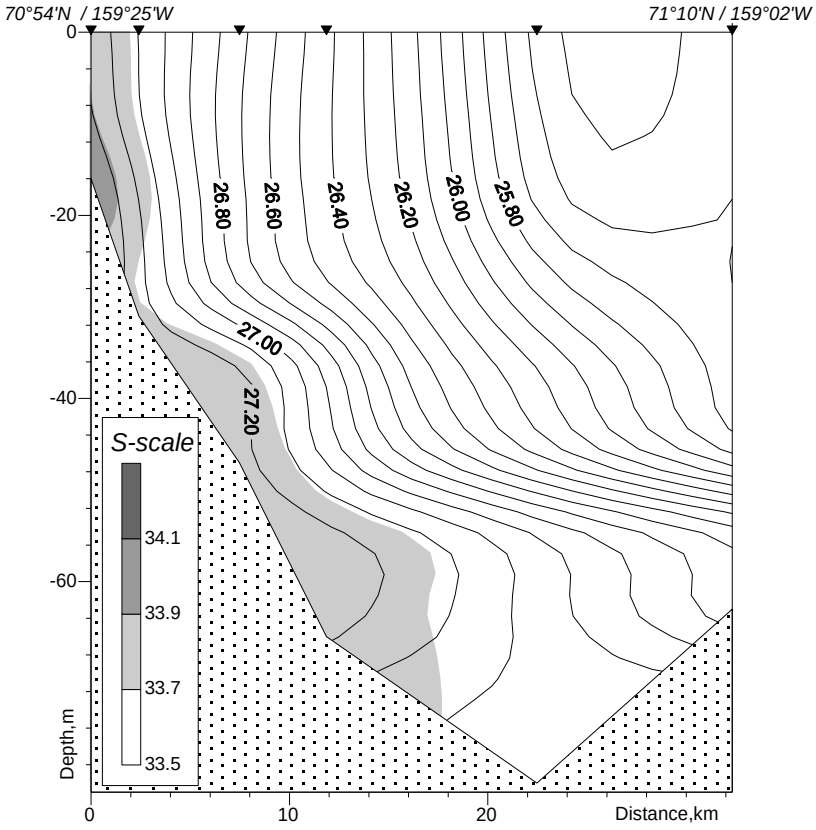
70°54'N / 159°25'W
71°10'N / 159°02'W
0
-20
-40
-60
Depth,m
26.80
26.60
26.40
26.20
26.00
25.80
27.00
27.20
S-scale
34.1
33.9
33.7
33.5
0
10
20
Distance,km

Fig. 10

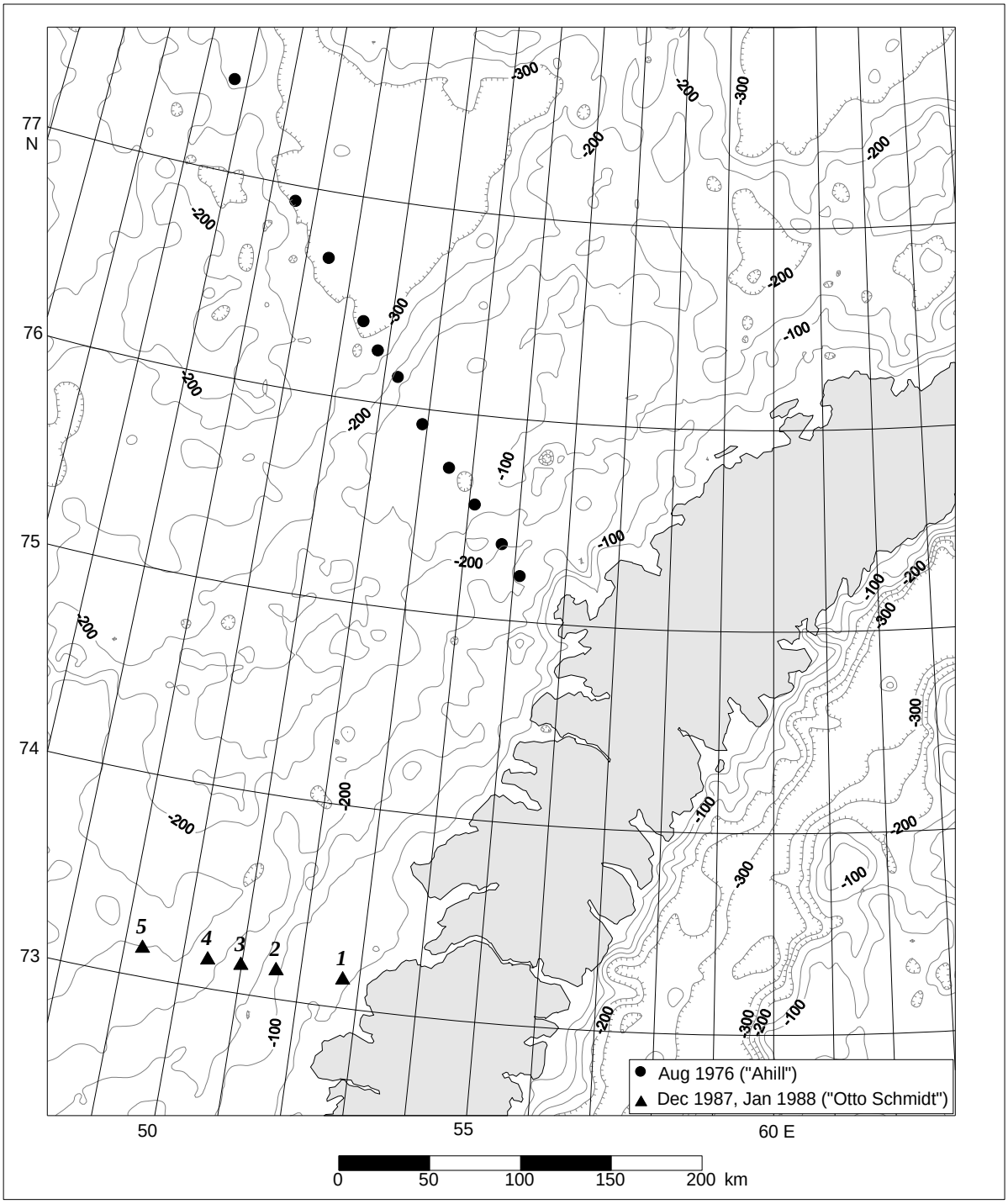
77
N
76
75
74
73
50
55
60 E
0
50
100
150
200 km
1
2
3
4
5
Aug 1976 ("Ahill")
Dec 1987, Jan 1988 ("Otto Schmidt")

Fig. 11

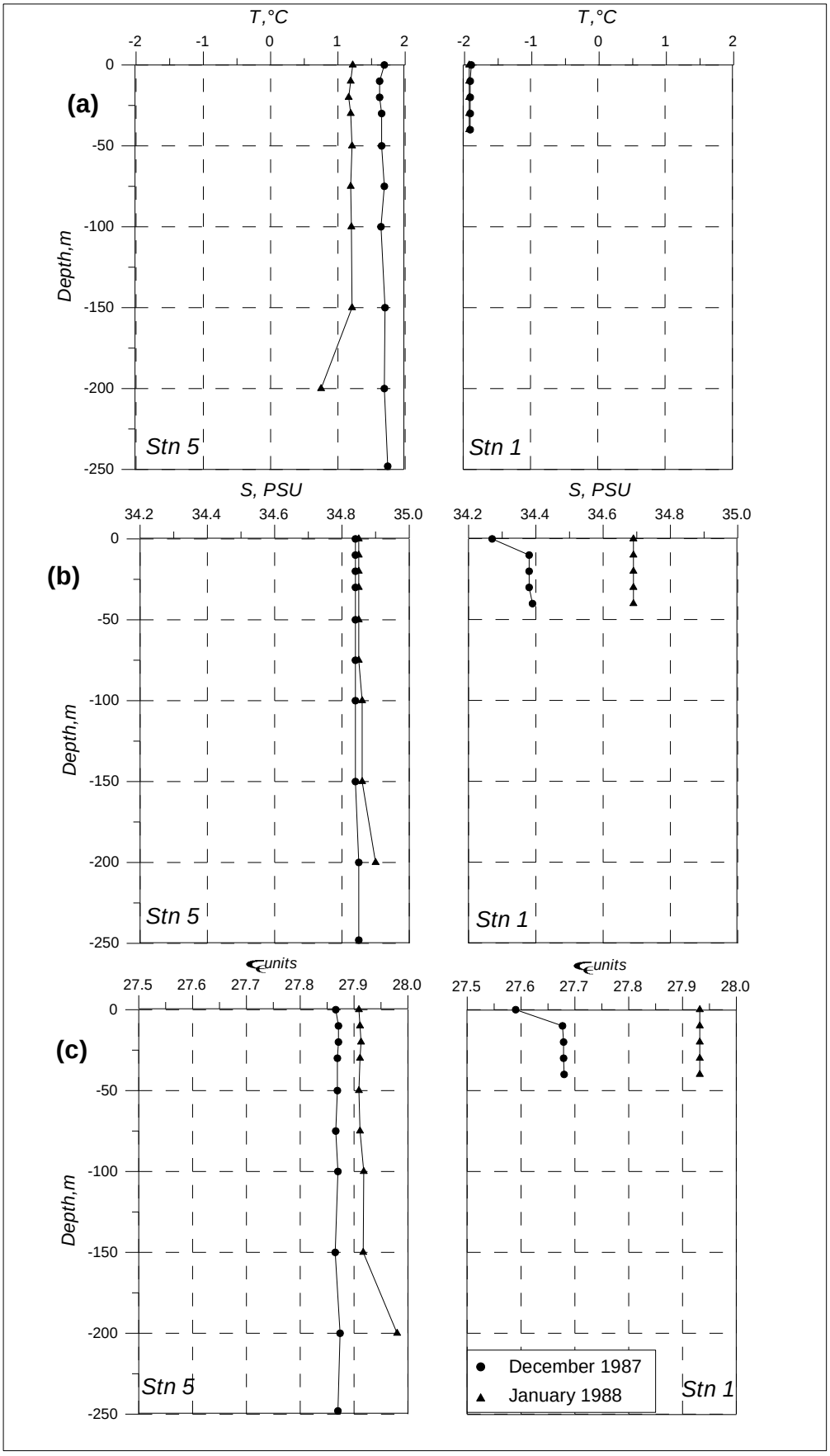
T,°C
-2
-1
0
1
2
(a)
0
-50
-100
-150
-200
-250
Depth,m
Stn 5
Stn 1
S, PSU
34.2
34.4
34.6
34.8
35.0
(b)
Stn 5
Stn 1
σt units
27.5
27.6
27.7
27.8
27.9
28.0
(c)
Stn 5
Stn 1
December 1987
January 1988

Fig. 12

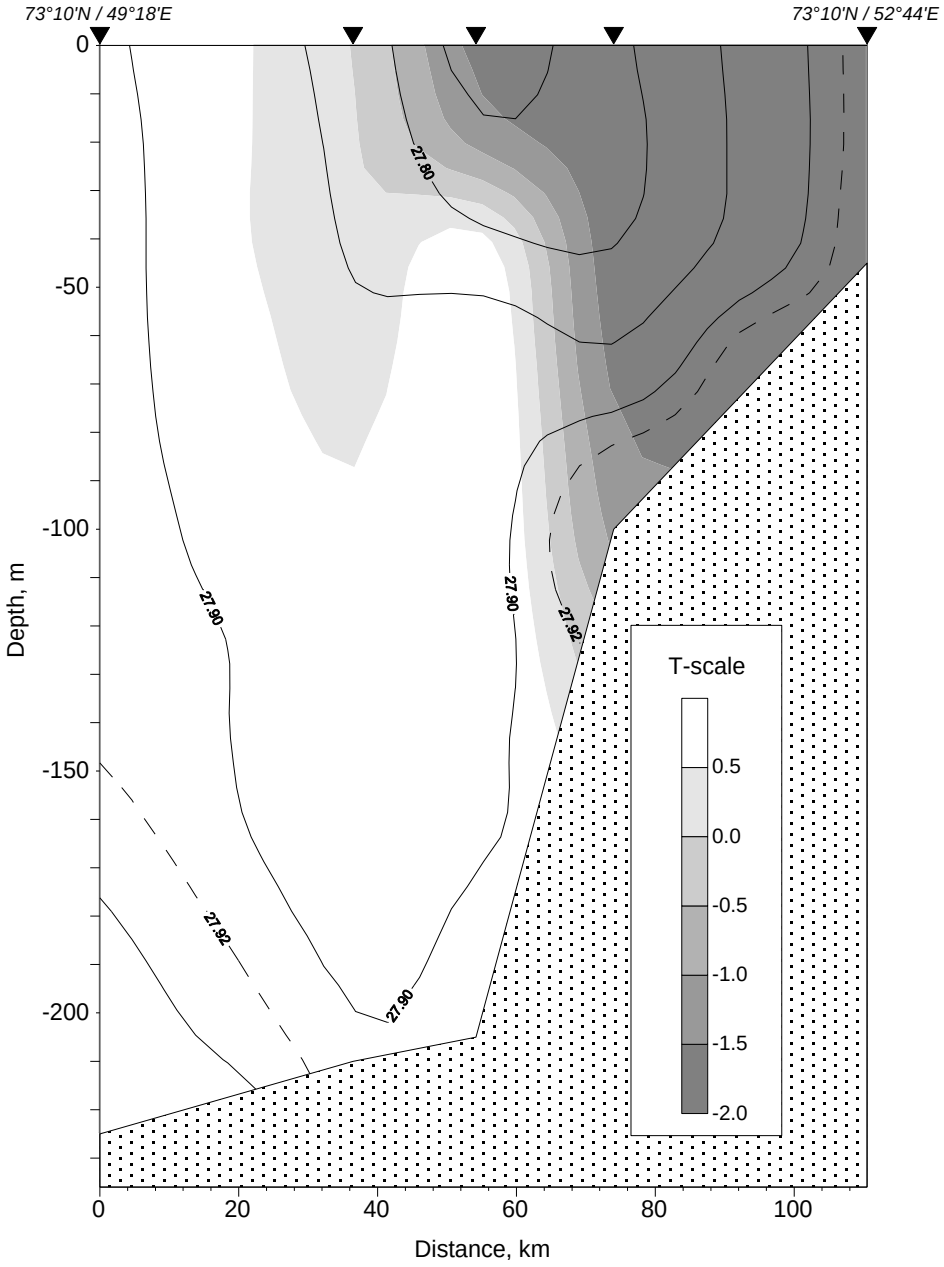
73°10'N / 49°18'E
73°10'N / 52°44'E
0
-50
-100
-150
-200
Depth, m
27.90
27.92
T-scale
0.5
0.0
-0.5
-1.0
-1.5
-2.0
0
20
40
60
80
100
Distance, km

Fig.13-a

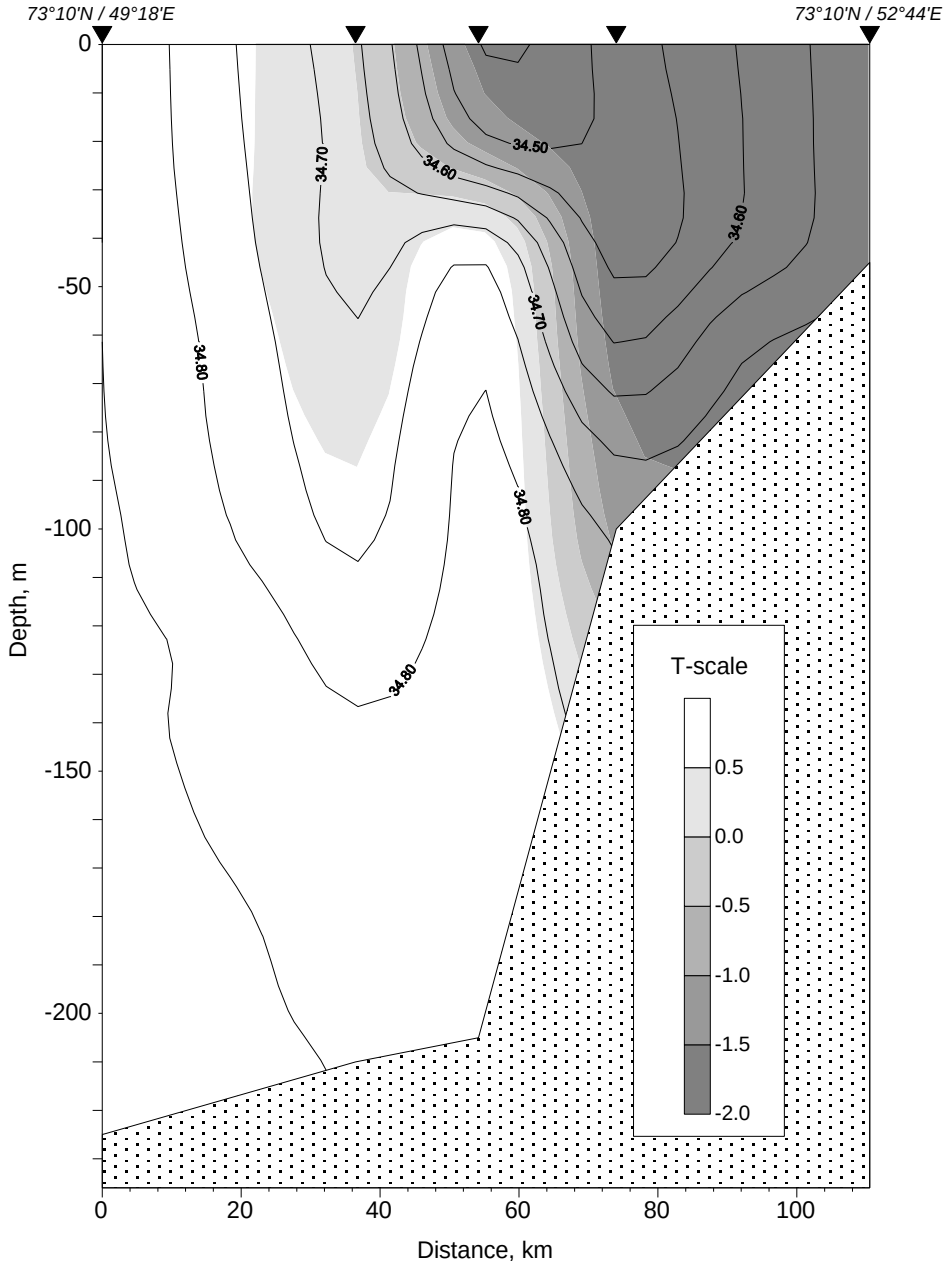
73°10'N / 49°18'E
73°10'N / 52°44'E
0
-50
-100
-150
-200
Depth, m
0
20
40
60
80
100
Distance, km
34.50
34.60
34.70
34.80
T-scale
0.5
0.0
-0.5
-1.0
-1.5
-2.0

Fig. 13-b

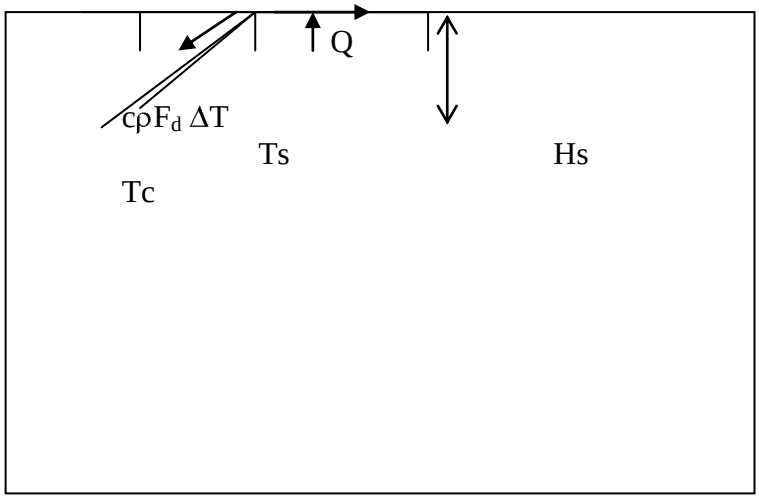

Fig. 14

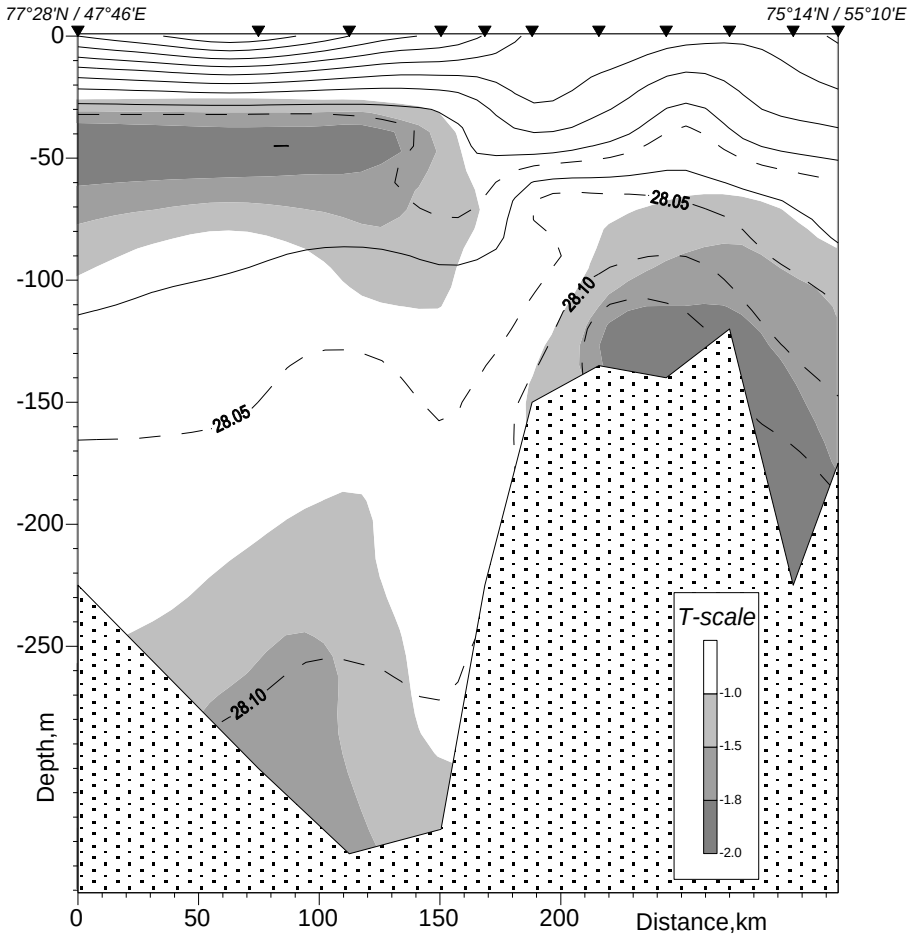
77°28'N / 47°46'E
75°14'N / 55°10'E
0
-50
-100
-150
-200
-250
Depth,m
28.05
28.10
28.05
28.10
T-scale
-1.0
-1.5
-1.8
-2.0
0
50
100
150
200
Distance,km

Fig. 15